# Middle Paleozoic convergent orogenic belts in western Inner Mongolia (China): framework, kinematics, geochronology and implications for tectonic evolution of the Central Asian Orogenic Belt

Bei Xu, Jacques Charvet, Yan Chen, Pan Zhao, Guanzhong Shi

# Middle Paleozoic convergent orogenic belts in western Inner Mongolia (China): framework, kinematics, geochronology and implications for tectonic evolution of the Central Asian Orogenic Belt

Bei Xu[a]

Jacques Charvet[b]

Yan Chen[b]

Pan Zhao[a]

Guanzhong Sh[a]

[a] Key Laboratory of Orogenic Belts and Crustal Evolution, Ministry of Education, Peking University, Beijing, 100871, China

[b] Institut des Sciences de la Terre d'Orléans, UMR 7327 Université d'Orléans-INSU/CNRS, 1A rue de la Férollerie, 45071 Orléans, Cedex 2, France

## Abstract

Based mainly on field geological observation and geochronologic data, six tectonic units have been recognized in western Inner Mongolia (China), including, from south to north: North China Craton (NCC), Southern Orogenic Belt (SOB), Hunshandake Block (HB), Northern Orogenic Belt (NOB), South Mongolia microcontinent (SMM), and Southern margin of Ergun Block (SME), suggesting that the tectonic framework of the CAOB in western Inner Mongolia is characterized by an accretion of different blocks and orogenic belts. The SOB includes, from north to south, fold belt, mélange, arc-pluton belt, and retroarc foreland basin, representing a southern subduction–collision system between the NCC and HB blocks during 500–440 Ma. The NOB consists also of four units: arc-pluton belt, mélange, foreland molasse basin, and fold belt, from north to south, representing a northern subduction–collision system between the HB and SMM blocks during 500–380 Ma. From the early Paleozoic, the Paleo-Asian oceanic domains subducted to the north and the south, resulting in the forming of the SOB and the NOB in 410 Ma and 380 Ma, respectively. This convergent orogenic system, therefore, constrained the consumption process of the Paleo-Asian Ocean in western Inner Mongolia. A double subduction–collision accretionary process is the dominant geodynamic feature for the eastern part of the CAOB during the early to middle Paleozoic.

## Keywords

Central Asian Orogenic Belt; Inner Mongolia; Paleo-Asian Ocean; Mélange, foreland basin

## 1. Introduction

The Central Asia Orogenic Belt (CAOB) is a giant accretionary orogen between the Siberian craton and the North China and Tarim cratons and is characterized by a series of island arcs, forearc or backarc basins, ophiolitic belts and microcontinents from the Neoproterozoic to Mesozoic (e.g., [Hsü et al., 1991], [Mossakovsky et al., 1993], [Sengör et al., 1993], [Sengör and Natal'in, 1996], [Badarch et al., 2002], [Khain et al., 2002], [Khain et al., 2003], [Xiao et al., 2003], [Buslovl et al., 2004], [Safonova et al., 2004], [Xiao et al., 2004], [Li, 2006], [Kröner et al., 2007], [Demoux et al., 2009a], [Xiao et al., 2009], [Kröner et al., 2010], [Xiao et al., 2010], [Glorie et al., 2011] and [Kröner et al., 2011]) and its massive generation of juvenile crust during the Phanerozoic ( [Hong et al., 1996], [Han et al., 1997], [Jahn et al., 2000a], [Jahn et al., 2000b], [Hong et al., 2004], [Jahn et al., 2009] and [Han et al., 2011]). Different evolutionary models have been suggested ( [Sengör et al., 1993], [Mossakovsky et al., 1993] and [Windley et al., 2007]).

Numerous recent regional studies show that the eastern segment of the CAOB is composed of a series of orogenic belts built from the Neoproterozoic to Mesozoic with several Precambrian microcontinental blocks between the Siberian and North China cratons (Fig. 1B; e.g., REFS). For example, a late Paleozoic active margin and an arc belt have been suggested in southern Mongolia ( [Yarmolyuk et al., 2005], [Yarmolyuk et al., 2008], [Bayaraa et al., 2010] and [Blight et al., 2010]), several Precambrian blocks and a huge late Pan-African metamorphic belt have been recognized in NE China ( [Zhou et al., 2009], [Zhou et al., 2010a] and [Zhou et al., 2011]), and a late Paleozoic Andean-style continental arc developed on the northern margin of the North China craton has been suggested ( [Zhang et al., 2007] and [Zhang et al., 2009a]). Western Inner Mongolia is part of the eastern segment of the CAOB, where the North China craton (NCC) is adjacent to the South Mongolian microcontinent (SMM). There are diverse ideas about the Paleozoic tectonic evolution. Xu and his co-workers ( [Xu and Chen, 1993], [Xu and Chen, 1997] and [Xu and Charvet, 2010]) suggested two opposite subductions and collisions during the middle Paleozoic to account for this evolution, emphasizing the late Devonian closure of the Paleo-Asian ocean along Ondor Sum in the south and Sunid Zuoqi in the north. [Chen et al., 2000] and [Chen et al., 2009] suggested long-lived multiple southward and northward subductions from 530 to 250 Ma until a collision between the Tuva-Mongolia microcontinent and NCC ranging from 296 to 234 Ma, based on their zircon U–Pb ages, Hf and Nd–Sr isotopic data. [Xiao et al., 2003] and [Xiao et al., 2009] took SHRIMP data from 300 Ma to 250 Ma from ultramafic rocks in Inner Mongolia as evidence of the Paleo-Asian Ocean and considered that an end-Permian to mid-Triassic termination of the accretionary processes resulted in the final amalgamation of the CAOB. [Jian et al., 2008] and [Jian et al., 2010] emphasized an early to mid-Paleozoic paired orogens and their evolution processes followed by a Permian intra-oceanic arc-trench system and a sequence of tectono-magmatic events from 299 Ma to 260 Ma responsible for the CAOB accretion, according to their detailed SHRIMP ages and geochemical data.

In this study we present the framework, kinematics and geochronology of a middle Paleozoic couple of convergent orogenic belts between the SMM and NCC in western Inner Mongolia of China, according to field observations and 1:50,000 geological mapping in key areas. We also present LA-ICPMS U–Pb ages in order to constrain the tectonic evolution of the belts. Based on these constraints and review of previous data, a tectonic evolutionary model of the convergent orogenic system and its implications for the tectonic evolution of the CAOB are also discussed.

## 2. Tectonic outline

Geologically, western Inner Mongolia belongs to the eastern part of the CAOB, which is characterized by the amalgamation of Paleozoic orogenic belts, Precambrian microcontinents and their margins (Fig. 1A and B). Six tectonic units can be identified in western Inner Mongolia, including the NCC, SMM, southern margin of the Ergun block (SME), Northern orogenic belt (NOB), Southern Orogenic Belt (SOB) and Hunshandake block (HB) between the NOB and SOB (Fig. 1C).

The NCC is characterized by an Archean-Paleoproterozoic metamorphic basement ( [Wan et al., 2011], [Zhai and Santosh, 2011] and [Geng et al., 2012]). It is called the Baoyintu Group in western Inner Mongolia, which includes quartzite, quartz rich micaschist, staurolite–kyanite schist intercalated with marble and plagioclase amphibole schist, dolomitic marble, staurolite–garnet mica schist, biotite bearing amphibole schist, leptynite and actinolite schist A whole rock Sm–Nd isochron age of 2485 ± 128 Ma from the plagioclase amphibole schist is interpreted as the age of the Baoyintu Group (IMBGMR (Inner Mongolian Bureau of Geology and Mineral Resources), 1991 and [Xu et al., 2000]).

The SMM is also called the Hutag Uul block or Totoshan Ulanul block in southwestern Mongolia (Badarch et al., 2002), extending ca. 600 km in E–W direction. It is represented in the Airgin Sum area, western Inner Mongolia, by the Airgin Sum Group, mainly composed of quartz rich micaschist, meta-volcanic rocks, meta-sandstone and marble (IMBGMR, 1991). An upper intercept age of 952 ± 8 Ma has been obtained from a two-mica gneissic granite of the Hutag Uul block (Yarmolyuk et al., 2005).

Extending from Erenhot in the west to Uliastai in the east, the 400 km long SME is composed of Ordovician and Devonian rocks, interpreted as the Paleozoic continental margin of the Ergun block (Xiao et al., 2003).

The HB may be considered as an independent tectonic unit between the NOB and SOB, unraveled by the Precambrian to early Cambrian detrital zircons from a mélange zone (see Sections 5.2). The HB sedimentary cover is represented by scattered outcrops of the Lower Paleozoic Ondor Sum Group and Upper Paleozoic limestone and clastic rocks (IMBGMR, 1991).

The NOB extends ca. 550 km from Xilinhot in the east to Airgin Sum in the west in our study area. Four units have been recognized (Fig. 2; [Xu et al., 1994] and [Xu and Chen, 1997]). Detailed observations of arc pluton have been reported by previous authors ( [Chen et al., 2000], [Shi et al., 2004a], [Shi et al., 2004b], [Shi et al., 2005], [Jian et al., 2008] and [Chen et al., 2009]).

The SOB extends from Ondor Sum, via Bater, to Tugurige, with a length of ca. 600 km from west to east. It has been defined based on detail studies of ophiolite, arc pluton, mélange, fold deformation and blueschist in the Ondor Sum and Bater areas ( [Shao, 1986], [Hu et al., 1990], [Tang, 1990], [Tang and Zhang, 1991], [Xiao et al., 2003] and [Jian et al., 2008]). Four units have been recognized in the Tugurige area (Fig. 8; Xu et al., 2001b).

## 3. Northern orogenic belt (NOB)

The NOB consists of four units from north to south: arc-pluton complex, mélange, molasse basin, and fold belt (Fig. 1C). The arc-pluton complex extends discontinuously in Airgin Sum, Baiyanbaolidao, and Xilinhot areas from west to east. The mélange can be discontinuously traced in Airgin Sum, Naomuhunni and Honger areas, from west to east. The molasse basin occurs near the mélange or arc-pluton complex to the south of Abag and Baiyanbaolidao. The fold belt crops out in the southern area (Fig. 2). In this section, the tectonic units are firstly described, and the configuration and polarity of the NOB will be then discussed according to available geometric and kinematic features in the fold belt and mélange.

### 3.1. Arc-pluton complex: a review of data

#### *3.1.1. Baiyanbaolidao area*

Three tectonic units of the NOB have been recognized in Baiyanbaolidao area, to the south of Sonid Zuoqi, arc-pluton complex, mélange, and molasse basin (Fig. 2; [Xu et al., 1994] and [Xu and Chen, 1997]).

Arc-pluton complex consists of cumulate gabbros, gabbro-diorites, quartz diorites, tonalites, granites and occurs in a wide area of ca. 20 × 6 km. These rocks were affected by greenschist-facies metamorphism and locally developed foliations. Geochemically, Nd-Sr and *In-situ* zircon Hf isotopic analyses indicate that the complex represents a subduction-related arc magmatic belt ( [Chen et al., 2000] and [Chen et al., 2009]) although a more complex evolution, from subduction to microcontinent accretion, has been proposed (Jian et al., 2008). Two U–Pb zircon ages of 418 and 439 Ma have been obtained from plagiogranite and granodiorite, respectively (Tang and Zhang, 1991) and another U–Pb zircon age of 418 ± 3 Ma from quartz diorite has been reported (Xu and Chen, 1997). Though two much younger ages of 309 ± 8 Ma and 310 ± 5 Ma have been interpreted as the forming age of the youngest arc ( [Chen et al., 2000] and [Chen et al., 2009]), more detailed geochronological data from eleven samples of cumulate gabbro (482.5 ± 1.7 Ma), quartz diorite (475 ± 6 Ma, 479.7 ± 1.8 Ma), tonalite (479 ± 8 Ma, 464 ± 8 Ma, 471.3 ± 2.4 Ma), biotite monzonitic granite (423 ± 8 Ma), biotite granite (424 ± 10 Ma) and granite (422.8 ± 1.9 Ma, 427.3 ± 2.2 Ma, 440 ± 4 Ma) suggest an early to mid-Paleozoic arc-pluton complex ( [Shi et al., 2004b], [Zhang et al., 2004], [Shi et al., 2005] and [Jian et al., 2008]).

#### *3.1.2. Other areas*

Jian et al. (2010) show that the SMM (Hutag Uul Block) in South Mongolia contains a metamorphic complex with orthogneiss (ca. 431 Ma) and amphibolite (ca. 477 Ma), suggesting the western continuation of the northern arc pluton complex. Yarmolyuk et al. (2005) report an age of 433 ± 12 Ma from one of the two-mica gneissic granites of this block. Several ages and geochemical results of biotite-plagioclase gneisses from the so-called Xilin Gol Complex in Xilinhot area, about 180 km to the east of Baiyanbaolidao, are reported. These gneisses, related to migmatization, yield detrital zircon ages of 437 ± 3 Ma and 452 ± 5 Ma and their geochemical features suggest a migmatization in a middle Paleozoic continental arc correlated with the arc pluton in Baiyanbaolidao area ( [Shi et al., 2003], [Li et al., 2010a] and [Li et al., 2010b]). The youngest zircon age is 406 ± 7 Ma, revealing the youngest arc magmatism (Xue et al., 2009). Ge et al. (2011) recently dated at ca.

411.0 ± 5.9 Ma (SHRIMP zircon age) the Lower Devonian volcanic rocks which unconformably overlay the Xilin Gol Complex, and at ca. 421 ± 1.8 Ma the granite which intrudes the Complex.

These new results suggest that the middle Paleozoic magmatic arc is composed of both volcanic rocks and plutons in Xilinhot.

### 3.2. Mélange belt

Our field survey shows that the Mélange belt occurs from Honger, Naomuhunni, to the south of Baiyanbaolidao, to Airgin Sum, marking a suture line of the NOB (Fig. 1C).

#### *3.2.1. Naomuhunni area*

The mélange extends more than 10 km in an ENE–WSW trend from Naomuhunni to Chaganwula in our mapping area (Fig. 2). The well-exposed mélange varies in width from 5 km in the west to 2 km in the east and consists of various blocks in heterogeneously deformed matrix. Blocks range from 0.2 m to 400 m in length. In decreasing order of abundance, these blocks include: dolomite (Fig. 3A), quartzite and limestone (Fig. 3B), ultramafic and mafic rock (Fig. 3C) and blueschist (Fig. 3E). For example, in an area of 240 × 140 m near Naomuhunni, 23 blocks are counted, made of dolomite, quartzite, limestone, ultramafic and mafic rock, and blueschist (Fig. 3D). Blueschist was only observed as isolated blocks of 10–20 m in width and 50 m in length, from which a Na-amphibole (Fig. 3E) Ar/Ar age of 383 ± 13 Ma has been obtained and interpreted as a high pressure metamorphic age (Xu et al., 2001a). Blocks of ultramafic and mafic rocks have been serpentinized, exhibiting strong schistosity and reaching more than 200 m in length and width (Fig. 3C). The matrix, in fault relationship with the blocks (Fig. 3F), consists of greenschist and sericite quartz schist and shows a highly penetrative deformation.

#### *3.2.2. Western and eastern extension*

200 km to the west of Naomuhunni area, with an outcrop of about 1 km × 10 km, the mélange belt in Airgin Sum area shows a geomorphologic landscape similar to that in Naomuhunni area, which is characterized by matrix in gentle relief and isolated blocks (Fig. 4A). The blocks include foliated dolomite (Fig. 4B), mafic rock (Fig. 4C) and granite (Fig. 4D). The matrix is made of green sericite quartz schist. The foliations in matrix and blocks are identically northwest-dipping.

The mélange belt extends to the Honger area, ca 50 km to the east of Naomuhunni, where there are several kinds of blocks, such as ultramafic rock, ferriferous quartzite, limestone in a matrix of green sericite quartz schist. Some blocks of ferriferous quartzite and limestone are so big that they are exploited as small mines.

### 3.3. Molasse basin

This unit occurs only in the Baiyanbaolidao, Honger and southern Abag areas. From Baiyanbaolidao a continuous succession can be observed.

### *3.3.1. Baiyanbaolidao area*

To the north of the mélange belt, sedimentary rocks of molasse basin, called the Seribayanobo Formation, occur in an area of about 2 km × 10 km. With a thickness of 691 m (Xu et al., 1994), it is characterized by red continental molassic sedimentary rocks distributed in two continuous sequences (Fig. 5A). The lower sequence comprises 229 m thick conglomerates and sandstones that can be divided into several cycles (Fig. 5F). The lower part of the each cycle is characterized by red and massive block-supported conglomerates intercalated with laterally discontinuous coarse-grained sandstones, in which massive bedding was observed. Gravels vary in composition and size, including rounded to sub-angular volcanic or plutonic rock, mica quartz schist, quartzite, and marble ranging from 2 to 20 cm in diameter (Fig. 5E). Containing plant fossils, such as *Leptophloeum rhombicum* (Shao, 1991), the sandstones are followed by 112 m thick grayish-green interbedded sandstones and siltstones, and then 40 m-thick argillaceous limestones in which several kinds of fossils, such as: *Nalivkinella profunda, Cyrtospirifer sulcifer*, have been found ( IMBGMR (Inner Mongolian Bureau of Geology and Mineral Resources), 1991 and [Xu et al., 1994]), belonging to the index fossils of the Late Devonian Famennian stage (374–359 Ma, Gradstein et al., 2004). The upper sequence comprises 411 m-thick sandstones interbedded with shales in the lower part (Fig. 5D), followed by 51 m thick argillaceous limestones in the upper part. It can be divided into several fining-upward cycles which contain sedimentary structures, such as ripple mark and inclined bedding (Xu et al., 1994). These sedimentary structures, along with those occurring in the overlying Lower Carboniferous Gouhudag and Nomgenhudag formations (Fig. 5C), display a southeastward paleocurrent trend (Fig. 5B), suggesting that the source area of the molasse basin was in the north during the late Devonian-early Carboniferous. Clasts in sandstones are largely composed of monocrystalline quartz grains and polycrystalline lithic fragments, which characterize plutonic and volcanic origins and imply a possible recycled orogen provenance (Dickinson, 1974).

There is a clear angular unconformity between the Upper Devonian and the underlying mélange (Fig. 5G and H), the Upper Devonian thick conglomerate unconformably overlies the sericite quartz schists of the mélange with north-dipping schistosity, indicating that the molasse basin developed after the formation of the mélange and that the unconformity is post-dating a pre-late Devonian deformation.

### *3.3.2. Other areas*

Molasse basin also occurs to the south of Abag and Honger (Fig. 1C), where the Upper Devonian sequence is composed of red thick sandstones and conglomerates in which sub-angular or angular granite gravels dominate, implying an erosion phase of the early Paleozoic arc plutons in the eastern part of the NOB (Tang and Zhang, 1991).

## 3.4. Fold belt

Exhibiting a greenschist-facies metamorphism and strong folding deformation, the fold belt occurs in an area of 6 km × 15 km to the south of the mélange and molasse basin in Baiyanbaolidao area (Fig. 2). The rock assemblage, called the Ondor Sum Group, is made up of sericite quartz schist, actinolite schist, and ferriferous quartzite intercalated with chert and marble lens (IMBGMR, 1991). 50 km and 200 km to the west, in Qagan Nur and Airgin Sum, respectively (Fig. 1C), the early Paleozoic Ondor Sum Group is also characterized by sericite quartz schists, showing folds at the outcrop scale (Fig. 6A). These discontinuous outcrops

trace the fold belt extending for 300 km that represents the northward-subducted passive margin of the HB during the early Paleozoic.

### 3.5. Kinematic analysis and configuration of the NOB

In the Baiyanbaolidao area, two deformational events are distinguished within the fold belt. The first event is characterized by centimeter-sized rootless folds that are not the main ones responsible for the regional structure. The second structural event is marked by south-verging slightly inverted folds ($F_2$) that are typically developed at the outcrop scale (Fig. 6A). Regionally, they are recognized by a widespread north-dipping foliation underlined by sericite, mica or quartz aggregates (Figs. 6B and inset in Fig. 2). Strong deformation is also found in the ophiolite mélange section where the foliation, observed in both matrix and serpentinized ultramafic rocks and blueschist blocks, shows a northwest or northeast dipping. These north-dipping foliations and south-inverted folds suggest a top-to-south kinematic direction.

In the Airgin Sum area, a ca. 3 km wide northwest-dipping ductily deformed granitic zone has been recognized with northwest-dipping foliations and stretching lineations (Fig. 6C). S–C fabrics, lenses and ribbons of recrystallized quartz and fragmented feldspar constitute top-to-the-southeast kinematic criteria (Fig. 6D). About 10 km to the south, the above-mentioned northwest-dipping mélange belt displays also identically northwest-dipping foliations with typical orientations of 320/66 and 334/36 for the gabbro (Fig. 4C) and granite (Fig. 4D) blocks, respectively. These features, together with the northward dipping schistosity in the mélange and axial-plane foliation in fold belt in the Baiyanbaolidao area, suggest a top-to-southeast kinematic sense.

Based on our 1:50000 mapping in the Baiyanbaolidao area (Xu et al., 1994), Fig. 7 shows a representative section summarizing the juxtaposition of four tectonic units including the arc-plutons complex, mélange, molasse basin and a fold belt, and indicating the configuration and polarity of the NOB. The latter is interpreted as due to a northward subduction of the northern margin of the HB.

## 4. Southern orogenic belt (SOB)

On the base of our 1:50000 mapping in Tugurige area (Fig. 8; Xu et al., 2001b) ca. 100 km to the west of Solonker and comparative observation in the Bater and Ondor Sum areas, four E–W-trending tectonic units of the SOB have been recognized in a 80 km × 800 km area (Fig. 1C). Composed of the early Paleozoic Ondor Sum Group, the fold belt is observed in both the Tugurige and Ondor Sum areas. The mélange belt is characterized by a south-dipping subduction–accretion complex that extends westwards from Ondor Sum ( [Hu et al., 1990], [Tang, 1992] and [Xiao et al., 2003]) and Bater to Tugurige areas. To the south of the mélange belt an arc magmatic belt including volcanic rocks and plutons can be traced from the Boin Sum, Bater (Jian et al., 2008) to Tugurige areas. To the south of the arc magmatic belt, an east–west trending foreland basin belt occurs in the Tugurige, Bater and Boin Sum areas, with flysch in the lower part and molasse in the upper part ( [Zhang and Tang, 1989], [Hu et al., 1990], [Tang, 1992], [Xu et al., 2001b] and [Zhang et al., 2010]). In this section, we describe the tectonic units in Tugurige and Bater areas and discuss the configuration and polarity of the SOB according to geometric and kinematic features of these units.

### 4.1. Mélange belt

The intensively deformed mélange belt is discontinuously cropping out between the fold belt in the north and the arc magmatic belt in the south from Tugurige, Bater, to Ondor Sum (Fig. 1C).

#### *4.1.1. Tugurige area*

There is a continuous exposure of the SOB within an area of ca. 20 km × 20 km in Tugurige area, where the four tectonic units have been recognized (Fig. 8; Xu et al., 2001b). Outcrops of the mélange discontinuously extend for 10 km along the E–W boundary between the fold belt in the north and the arc magmatic belt in the south in Ganqimaode, Tugurige area (Fig. 8). The largest outcrop can be sized up to 2 km × 4 km, where huge blocks appear as small hills (Fig. 9A). The matrix consists of greenschist and sericite quartz schist and shows a highly penetrative deformation and cataclastic texture (Fig. 9B). The most common texture in the mélange is matrix-supported blocks (Fig. 9C). Blocks range from 0.02 m to 30 m in size and are composed of ultramafic and mafic rocks (Fig. 9D), white mica schist (Fig. 9E), hornblende schist (Fig. 9F) and granite (Fig. 9C).

#### *4.1.2. Bater area*

A mélange belt discontinuously extends for ca. 40 km from Gangnaobao to Hongqimuchang in Bater area (Fig. 1C), characterized by "block mélange" or ductile deformation belt composed of deformed blocks of volcanic and sedimentary rocks. For example, several kinds of blocks have been observed along a 300 m long prospecting trench near Gangnaobao with a size ranging from several to 10 m in length, and variable lithologies, including ultramafic rock (Fig. 10A), gabbro, quartzite schist and granite. The ultramafic rock blocks have been serpentinized, with highly penetrative deformation and cataclastic texture (Fig. 10B). The quartz schists and granites occur as blocks of 40 m × 40 m with mylonitic (Fig. 10C) or cataclastic texture (Fig. 10D). As a westward extension of the mélange, a strong ductile deformation belt occurs to the south of Hongqimuchang where ductily deformed mylonitic schists, with small asymmetric folds (Fig. 10E), and pillow lavas have also been found (Fig. 10F). Composition of the mélange suggests a protolith formed as an accretionary wedge in a forearc setting.

#### *4.1.3. East of Ondor Sum: a review*

Several authors have described an ophiolitic mélange with intensive ductile deformation and blueschist facies metamorphism as part of a mélange belt in Tulinkai, in the east of Ondor Sum area. For example, Hu et al. (1990), Tang (1992) and Xiao et al. (2003) show the distribution, composition and ductile deformation of the Tulinkai-Wuyitai ophiolitic mélange belt which extends for ca. 40 km in E–W direction, sandwiched by the fold belt of the Ondor Sum Group in the north and the arc magmatic belt of the Boin Sum Group in the south. Three $^{39}Ar/^{40}Ar$ ages of 445.6 ± 15 Ma, 453.2 ± 1.8 Ma and 449.4 ± 1.8 Ma from glaucophane and phengite in blueschists have been published, suggesting a high pressure metamorphic event related to southward subduction ( [Tang, 1992] and [De Jong et al., 2006]).

### 4.2. Arc magmatic belt

This belt extends discontinuously for ca. 600 km from Tugurige in the west via Bater to Ondor Sum in the east.

#### *4.2.1. New geochemical data in Tugurige area*

A 16 km long volcanic belt can be traced in Tugurige area (Fig. 8). The largest outcrop of volcanic rocks is about 3 km × 4 km, where a 1261 m thick field section shows that this belt consists of basalts (65% of section thickness) with thin intercalated red and green cherts, diabases, dacites, rhyolites, and 32 m thick sandstones (Xu et al., 2001a). All rocks are slightly metamorphosed and deformed.

To the south of the volcanic belt, a nearly continuous diorite belt intrudes into the Ordovician Baiyunshan Formation composed of foliated metasandstones and limestones. The E–W trending diorites develop south-dipping foliations and underwent low grade metamorphism, with a secondary mineral assemblage of chlorite + albite. The main mineral assemblage is made of plagioclase + hornblende + quartz ± microcline ± biotite ± white mica. Accessory minerals include sphene, apatite, zircon and magnetite. Three samples (Fig. 8, Bp9b2-5, Bp9b3-1, Bp9b1b) from the diorite belt show contents of $SiO_2$ = 53.62–54.91% and $K_2O$ = 1.56–1.80%, consistent with high to medium K calc-alkaline series (Table 1). Their REE patterns are characterized by the absence of Eu anomalies and low total REE. They also have $Y$ = 23.8–31.6 ppm and low $(La/Yb)_n$ ratio (3.40–4.37) shown in Fig. 11A. The primitive mantle-normalized spidergram (Fig. 11B) for these diorites exhibits strong LILE enrichment, negative HFSE anomalies, such as Nb, Ta, Zr, P and Ti. These diorite samples plot into the VAG field in a geochemical-tectonic discrimination diagram of Rb versus Y + Yb (Fig. 11C; Pearce, 1984), providing evidence for arc-related plutonism.

#### *4.2.2. New geochronology data in Tugurige area*

Based on the analysis of cathodoluminescence (CL) images (Fig. 11D), two zircon samples from quartz diorites in Tugurige area (BP9B1 and BP5B1, Fig. 8) were analyzed by LA-ICPMS and their results are presented in Table 2. Of thirty zircons of BP9B1, 27 zircons are concordant or nearly concordant. These 27 zircons mostly vary from 464 to 436 Ma, with a weighted mean $^{206}Pb/^{238}U$ age of 453.0 ± 5.1 Ma (MSWD = 0.68, Fig. 11E). Because they are euhedral with oscillatory zones in CL images (Fig. 11D) and have Th/U ratios from 0.33 to 0.57 (Table 2), indicating a magmatic origin (Hanchar and Rundnick, 1995), the $^{206}Pb/^{238}U$ age of 453.0 ± 5.1 Ma is interpreted as the formation age of sample BP9B1. Only one grain has $^{206}Pb/^{238}U$ age of 617 ± 6 Ma with a Th/U ratio of 0.99 (BP9B1-03, Table 2).

The dating of thirty zircons from BP5B1 shows concordant or nearly concordant results. They vary from 440 to 412 Ma, with a weighted mean $^{206}Pb/^{238}U$ age of 425.3 ± 3.1 Ma (MSWD = 2.6, Fig. 11F). These zircons are long prismatic grains with well developed oscillatory zoning in CL images (Fig. 11D), and have Th/U ratios from 0.23 to 0.66 (Table 2), indicating a magmatic origin, so the $^{206}Pb/^{238}U$ age of 425.3 ± 3.1 Ma is interpreted as the formation age of BP5B1. These two ages provide constraints to the upper and lower limits of the arc pluton magmatism in Tugurige area, and can correlate roughly with those in the Bater and Ondor Sum areas ( [Jian et al., 2008] and [Zhang and Jian, 2008]).

These ages, together with the geochemical data of volcanic rocks and plutons in the Tugurige area, imply that the early middle Paleozoic arc magmatic belt of the SOB extends from the Ondor Sum to Tugurige areas.

#### *4.2.3. Review of data from Bater and Ondor Sum areas*

Geochemical features in the Tugurige area are shared by the diorites in Bater and Ondor Sum areas about 200 km and 350 km to the east, respectively. Detailed geochemical results and SHRIMP data of arc magmatic belt from Bater area have been recently published ( [Jian et al., 2008], [Zhang and Jian, 2008] and [Li et al., 2010a]). Arc plutons consist of diorites and granites, and yield SHRIMP zircon ages of 453 ± 3 and 446.8 ± 5.3 Ma (Li et al., 2010a). A detailed time scale for the arc evolution has been presented, illustrating a magmatic stage linked to subduction during 497–450 Ma, and an anatexis stage during 451–436 Ma, according to the studies in southwestern Bater ( [Xu et al., 2003], [Jian et al., 2008] and [Zhang and Jian, 2008]). These observations lead us to link the arc magmatic belt in Bater with that in Tugurige areas as an E–W extending arc magmatic belt.

To the east, the middle Paleozoic arc magmatic belt characterized by volcanic rocks and plutons has been recognized by field and geochemical investigations in the Ondor Sum area ( [Hu et al., 1990], [Tang, 1992] and [Jian et al., 2008]). With a thickness of 810 m, the volcanic rocks, called the Boin Sum group, contain tholeiites, andesites, dacites, rhyolites and tuffs. Four zircon SHRIMP ages of 436 ± 9 Ma, 459 ± 8 Ma, 453 ± 7 Ma and 474 ± 7 Ma from the dacites and rhyolites of the Boin Sum group, have been obtained ( [Liu et al., 2003] and [Zhang, 2010]). The plutons in the Boin Sum area consist of granodiorite porphyry, granodiorite and quartz diorite with zircon ages of 466 Ma, 467 ± 13 Ma ( [Tang, 1992], [Liu et al., 2003] and [Chen et al., 2009]). A model of magmatic evolution from birth, youth, to maturity of the arc between 500–438 Ma has been proposed (Jian et al., 2008). The youngest pluton is dated at 430 ± 6 Ma (Chen et al., 2009), providing a constraint for the upper limit of the arc magmatism in the Boin Sum area.

### 4.3. Foreland basin belt

Foreland basin belt can be traced in Tugurige, Bater and Ondor Sum areas, extending more than 600 km in length (Fig. 1C), including a lower part composed of the Silurian flysch in Tugurige and Ondor Sum areas, and an upper part, the lower Devonian molasse in Bater and Ondor Sum areas, respectively. Paleogeographically, because the forearc accretionary wedge represented by mélange belt is to the north and the arc magmatic belt is to the south, the foreland basin belt can be seen as a retroarc foreland basin belt following Dickinson's classification (1974).

#### *4.3.1. Lower part of the foreland basin*

The Silurian flysch strata are continuously exposed in a 6 km × 20 km area between Tugurige and Ganqimaode (Fig. 8) and extend westwards and eastwards for tens of kilometers, respectively (IMBGMR, 1991). The flysch strata, called the Xuniwusu Formation with a thickness up to 7.4 km (Xu et al., 2001b), can be divided into a lower “canal facies”, characterized by coarse cycles of conglomerates, pebble-sandstones, sandstones, and a upper “fan facies” composed by sandstones and shales (Walker, 1979). There is a clear angular unconformity between the Xuniwusu Formation and the underlying Ondor Sum Group (Fig. 12A), where the thick conglomerate of the Xuniwusu Formation unconformably overlies

the sericite quartz schist of the fold belt with south-dipping schistosity, indicating that the foreland basin developed after the fold belt formation. In the lower part, thickness of coarse cycles ranges mostly from ca. 1 to 5 m and displays upward fining feature (Fig. 12B), with 0.5 to 4 m thick conglomerate beds. Clasts consist of poorly-sorted, subangular or subrounded schist, granite, volcanic rock and quartzite, ranging from 2 to 30 cm in diameter. The interbedded sandstones and siltstones, with 10–20 cm thickness, comprise Bouma sequences. These lithofacies characters are similar to those of Walker's (1979) "canal facies", which most likely deposited during an early phase of development of submarine fan along the northern continental margin of the NCC. The upper part of the flysch is characterized by continuous development of typical Bouma sequences that consist of sandstones and shales (Fig. 12C). With a change from 10 to 30 cm thick $T_{ae}$ in the base to 2–5 cm thick $T_{de}$ in the top, these Bouma sequences display upward fining cycles (Fig. 12D), suggesting a developing stage of submarine "fan facies" (Walker, 1979).

According to previous work, unconformably overlying the arc magmatic belt of the Boin Sum Group, the lower part of the foreland basin consists of the 1105 m-thick Xuniwusu Formation flysch in the Ondor Sum area ( [Hu et al., 1990] and [Tang, 1992]). With typical Bouma sequences and a lot of magmatic detritus, the flysch indicates a turbiditic sedimentation resulted from fast uplift of the arc magmatic belt. Flute casts in the flysch show paleocurrent of 145–150° SE (Hu et al., 1990), implying that the provenance of the Xuniwusu Formation flysch is the arc magmatic belt of the Boin Sum Group to the north.

#### *4.3.2. Upper part of the foreland basin*

As the upper part of the foreland basin, the Upper Silurian–Lower Devonian strata, called the Xibiehe Formation, are characterized by molasse and unconformably overlay the flysch succession, middle Paleozoic arc magmatic belt, mélange or fold belt ( [Hu et al., 1990], [Tang, 1992] and [Zhang et al., 2010]). For example, the Xibiehe Formation consists of > 339 m-thick molasse succession containing three conglomerates—sandstones cycles (Fig. 12E) in the lower part and several sandstones–shale–limestones cycles in the upper part in Bater area. With a thickness of up to 10 m, the conglomerates are red, poorly sorted and dominated by subangular clasts of volcanic rock, quartz vein, schist and carbonate (Fig. 12F). Above the conglomerates the red molasses displays 5–15 m thick cycles from clast-bearing sandstones to sandstones.

The Xibiehe Formation comprises a 924 m-thick molasse succession of conglomerates and sandstones and unconformably overlays the Xuniwusu Formation flysch or Ondor Sum Group in southern Ondor Sum ( [Hu et al., 1990] and [Zhang et al., 2010]). The conglomerates contain clasts of volcanic rock, quartz vein, granite and sericite quartz schist (Fig. 12G). Middle-sized inclined beddings can be observed in thick sandstone (Fig. 12H).

### 4.4. Fold belt

The fold belt composed of the southern margin of the HB can be found in both Tugurige and Ondor Sum areas. With an area of 4 km × 16 km, the fold belt occurs across the boundary between China and Mongolia in Tugurige area (Fig. 8). Called also the Ondor Sum Group, it is made up of sericite quartz schist, actinolite schist and ferriferous quartzite (IMBGMR, 1991). Three events of deformation are distinguished in the fold belt (Xu et al., 2001b). The first event is characterized by the penetrative foliations that completely displace beddings ($S_1$ in Fig. 13A), involved in outcrop- to kilometer-scale folds during the second structural event

(Fig. 13B). Regionally, these folds are cut by zonal crenulation cleavage of the third structural event, forming 2–10 cm-thick microlithons (Fig. 13C).

Similar deformational features are discovered in the Ondor Sum Group in the Ondor Sum area, and three deformation stages have been recognized in sericite quartz schist, actinolite schist and ferriferous quartzite (Hu et al., 1990). Among them, the second stage forms an E–W trending fold belt extending for 40 km and is considered as the main event responsible for the regional structure.

### 4.5. Configuration and polarity of the SOB

#### *4.5.1. Analysis of deformation of the foreland basin in Tugurige area*

The flysch of the Xuniwusu Formation forms northward overturned folds (Fig. 13D) with middle to high angle southward-dipping axial-plane cleavages ($S_1$) that cut bedding ($S_0$ in Fig. 13E). Specially, these axial-plane cleavages are more penetrative in siltstones and mudstones than in sandstones, but they do not displace beddings and sedimentary structures of the Bouma sequence, such as the graded bedding is maintained (Fig. 13F), which is different from foliations developed in the Ondor Sum Group. Regionally, these folds and southward-dipping axial-plane cleavages are widespread and easily observed in the Xuniwusu Formation, indicating the continuous north-inverted fold style. Both these folds and cleavages imply a top-to-north kinematic direction in the flysch of foreland basin.

#### *4.5.2. Deformation in Ondor Sum area: a review*

Detailed fold deformation study was conducted by Hu et al. (1990) in the Ondor Sum area. Three stages of folding occurred in the arc magmatic belt composed by the Boin Sum Group. Among them, the second stage folding is characterized by isoclinal or north-inverted folds at a regional scale and controls distribution of the Boin Sum Group. Regionally, axial plane foliation of the second folding is penetrative, stably southwest-dipping, indicating a top-to-northeast kinematic direction in the Boin Sum Group of the arc magmatic belt (Hu et al., 1990). Zeng (1990) studied the ductile deformation of several deformed zones with a width of several hundred meters developed in both the Boin Sum Group and Xuniwusu Formation; the kinematic indicators include south-dipping mylonitic schistosity, quartz and feldspar asymmetric pressure shadows, sheath-like folds, from which a top-to-north shearing sense has been deduced.

#### *4.5.3. Configuration and polarity of the SOB*

Fig. 14 shows a representative section summarizing the spatial relationship of four tectonic units in the Tugurige area as well as the configuration of the SOB, according to the data provided by Xu et al. (2001b). This section, together with the top-to-north kinematic features from these units, suggests a southward subduction of the southern margin of the HB beneath the NCC.

## 5. Discussion

### 5.1. Devonian molasse in the NOB: source area and significance

The Devonian succession occurs to the south of Baiyanbaolidao, Abag, and Hegengshan areas in the NOB (Fig. 1C). It has been known for twenty years that the Devonian continental sequence is characterized by typical red conglomerates and sandstones, with plant fossils (IMBGMR, 1991), but there are different interpretations for these continental clastic rocks. For example, the continuous Upper Devonian to Lower Carboniferous sedimentary succession overlying unconformably the mélange in the NOB is considered as a block evolved in the Solonker suture zone ( [Chen et al., 2000] and [Xiao et al., 2003]) or as the result of a local transgressive event (Li, 2006). However, a clear unconformity (Fig. 5H) between the Devonian continental molasse containing plant fossils and mélange containing blueschist block with the age of 383 Ma (Xu et al., 2001a) indicates the occurrence of a middle Paleozoic orogenic belt.

In order to reveal the source area and significance of the molasse, a sample (71108) of red sandstone from the lower part of the Seribayanobo Formation in Baiyanbaolidao area (Fig. 2) was analyzed by LA-ICPMS and its zircon Cathodoluminescence (CL) images are shown in Fig. 15A. All 75 zircon spots are concordant or nearly concordant (Fig. 15B) and their results are presented in Table 3. They show one major group including 66 zircon grains from 442 to 525 Ma with a peak value of 461 Ma (Fig. 15B), suggesting a major contribution of the provenance materials to the sediments. With Th/U ratios from 0.36 to 1.17, these zircons are euhedral to subhedral crystals, and their CL images show oscillatory zoning (Fig. 15A), indicating that they are of igneous origin. Other 8 grains show two groups of 906–1059 and 1338–1571 Ma in age, respectively, indicating a contribution of the late to middle Proterozoic source material. The oldest zircon shows an age of 2729 Ma. Being of igneous origin and making up 85% of all zircons, the dominant zircon age group with the peak value of 461 Ma reveals an erosion process of the early to middle Paleozoic arc magmatic belt. The youngest zircon age is 442 ± 6 Ma, suggesting that the deposition of this red sandstone could not be older than the earliest Silurian.

Geographically, the molasse basin where Sample 71108 is taken is near the early Paleozoic arc magmatic belt to the north and shows a southeastward paleocurrent trend (Fig. 5B), which implies a geographical relationship between these two units. Two groups of 906–1059 and 1338–1571 Ma are similar to the published ages of 954–983 Ma from the Baga Bogd massif in South Mongolia to the north ( [Demoux et al., 2009a] and [Demoux et al., 2009b]), and 916 ± 2 Ma and 952 ± 8 Ma from South Mongolia microcontinent to the west ( [Wang et al., 2001] and [Yarmolyuk et al., 2005]) and peak ages of 1348 and 1467 Ma of Mongolia to the north (Rojas-Agramonte et al., 2011). Considering the southeastward paleocurrent trend, this similarity implies that there was a late and middle Proterozoic block in the northwest, being the provenance of the Devonian red sandstone. Generally, the zircon age distribution pattern of Sample 71108 reveals that the early to middle Paleozoic arc magmatic belt is a pronounced source area and the late and middle Proterozoic block in the northwest maybe a subordinate source area for the molasse basin in the NOB during the late Devonian, implying an uplift and erosion process during post-collisional stage and giving a sedimentary constraint to the middle Paleozoic orogenic belt.

### 5.2. About the Hunshandake block

If there was the HB between the NOB and SOB, its nature is important to reveal the configuration of the middle Paleozoic convergent orogenic belt. There are scattered outcrops of the Ondor Sum Group around the Hunshandake Desert (Fig. 1C), they represent the continental margin of the HB and subducted ocean crust. A sample (71006, Fig. 2) from the mélange matrix that consists of the Ondor Sum Group was analyzed by LA-ICPMS to deduce composition and age of HB.

Its zircon Cathodoluminescence (CL) images are shown in Fig. 15A and probability plots of zircons in Fig. 16A. Of 75 zircon spots, 63 spots are concordant or nearly concordant and their results are presented in Table 3. Most zircons are subrounded and divided into three types according to CL imaging. Type A shows clear oscillatory zoning (71006–4, 71006–46), type B wider and obscurer oscillatory zoning (71006–2, 71006–63) and type C no oscillatory zoning (71006–53, Fig. 15A). Type A and B show Th/U ratios from 0.12 to 2.62, indicating an igneous origin, but type C, including spots 71006–21, 71006–33 and 71006–53, has Th/U ratios from 0.04 to 0.07, implying a metamorphic origin. Seven age groups have been recognized from the 63 spots (Fig. 16A), including 3258–2916 Ma (2 spots), 2558–2480 Ma (4 spots), 2189–2001 Ma (3 spots), 1830–1691 Ma (4 spots), 1302–1394 Ma (3 spots), 1220–903 Ma (27 spots), and 737–515 Ma (20 spots). The four older age groups indicate a contribution of the Archean to early Proterozoic source material, and are very similar to the age distribution of the NCC that is characterized by peaks of 3324, 2500, 2173 and 1800 Ma, representing granite-greenstone and TTG suite development and consolidation of the Archean blocks in the NCC (Fig. 16C, [Zhao et al., 2001], [Zhao et al., 2002], [Wilde et al., 2002], [Darbya and Gehrels, 2006], [Yang et al., 2006] and [Rojas-Agramonte et al., 2011]). The group of 1302–1394 Ma (3 spots) may be correlated with a rifting event which occurred in the northern margin of the NCC at around 1.35 Ga (Zhang et al., 2009b). These results imply that a block probably rifted from the NCC was the provenance area for the protolith of mélange.

Making up 75% of all analytical spots, the appearance of prominent groups of 737–515 Ma (20 spots) and 1220–903 Ma (27 spots) with six peaks at 576, 638, 735, 911, 973, and 1044 Ma is the most striking feature in this sample. This age distribution is different from that of other known tectonic units, such as the NCC to the south and SMM to the west ( [Cope et al., 2005], [Darbya and Gehrels, 2006], [Rojas-Agramonte et al., 2011] and [Wan et al., 2011]), and Mongolia or Xing-Meng Orogenic Belt to the north ( [Shi et al., 2003], [Chen et al., 2009], [Xue et al., 2009], [Li et al., 2010b] and [Li et al., 2011]). For example, the peaks at 576, 638 and 735 Ma marking the latest Precambrian magmatic event in the HB (Fig. 16A) have not been found in Mongolia (Fig. 16B). Conversely, two peaks at 815 Ma and 515 Ma reflecting early Neoproterozoic and early Paleozoic magmatic activities during the early stage of CAOB evolution in Mongolia plot (Fig. 16B; Rojas-Agramonte et al., 2011) do not occur in the HB (Fig. 16A).

These differences imply that there also was a latest Proterozoic magmatic provenance area for the protolith of mélange which was never recognized up to now. This novel source area, together with the above-mentioned Archean to early Proterozoic source area, leads us to deduce that there was an unknown block between the NOB and SOB, namely the Hunshandake block (HB), characterized by the NCC affinity and the latest Proterozoic and early Cambrian magmatism. It is the HB that supplied detrital materials for the protolith of mélange before a middle Paleozoic northward subduction.

Geographically, 20 km to the south of the sampling locality for 71006, there is an area which extends 600 km in E–W and 50–150 km in N-S between the NOB and SOB (Fig. 1C); its eastern part is occupied by the Hunshandake Desert, and its western part by sparse outcrops of the Paleozoic sequence. Therefore, it seems reasonable to suggest the existence of this block in this huge area.

### 5.3. The late Paleozoic tectonic evolution in western Inner Mongolia

There has been a debate about the late Paleozoic tectonic evolution in western Inner Mongolia for a long time. For example, another explanation of the arc-pluton complex of the NOB in Baiyanbaolidao area is that it represents products of a prolonged period of arc magmatism that developed on the southern margin of the SMM in the period 530–296 Ma ( [Chen et al., 2000] and [Chen et al., 2009]). Also, based on SHRIMP ages of Permian-early Triassic ultramafic-mafic rocks and their geochemistry, an intra-oceanic arc-trench system with multiple southward and northward subductions from 530 to 250 Ma, and a late Permian to middle Triassic collision along the Solonker suture zone have been proposed to describe the end-Paleozoic to mid-Triassic tectonic evolution in western Inner Mongolia ( [Chen et al., 2000], [Xiao et al., 2003], [Jian et al., 2008], [Chen et al., 2009], [Xiao et al., 2009] and [Jian et al., 2010]). Following these data, the Inner Mongolian orogenic belt is a long-lived one and a Permian wide ocean would have occurred between the SMM and NCC.

Several papers have reported occurrence of the late Paleozoic mafic rocks related to extensional rifting setting, bimodal volcanic suite, A-type granite (Fig. 1C). Chen et al. (2012) reported new data of geochronology (279–274 Ma) and geochemistry of Permian mafic rocks in Mandula area and suggested that they were emplaced in an extensional rifting setting and that Solonker belt probably represented a Red Sea-like ocean basin. Tang et al. (2011) recognized a Late Carboniferous bimodal volcanic suite (313308 Ma) from the western part of the HB, and suggested that it formed in an extensional setting after collision between the NCC and SMM. Shi et al. (2004a) found an A-type granite with an age of 276 Ma near Xilinhot and proposed that it represents post-collision magmatism. These studies imply that a wide oceanic lithosphere has not existed between the NCC, HB, and SMM after ca. 280 Ma, identically to studies from a wider area of the CAOB ( [Hong et al., 1996], [Hong et al., 2004] and [Jahn et al., 2009]).

Generally, to decipher the late Paleozoic tectonic evolution in western Inner Mongolia, two key questions are most worthy of being considered: what is the nature of the Permian sea area in western Inner Mongolia: a wide ocean, relict sea, or Red sea-type basin? Where is an integrated Permian-early Triassic orogenic belt like the early-middle Paleozoic orogenic belt? Obviously, the conclusion about the late Paleozoic tectonic evolution in western Inner Mongolia needs detailed study and more evidence.

### 5.4. Relationship between the SMM and SME

The relationship between the SMM and SME is unclear. One key problem is the age and tectonic setting of Hegenshan ophiolite representing the boundary between the two units. Robinson et al. (1999) deduced that the petrological characteristics are consistent with formation in an arc/back arc setting, probably in middle to late Devonian time. Miao et al. (2007) suggested that it represents a back-arc basin opened on a pre-Permian basement at ca. 295 Ma (Fig. 1C). These data imply that a late Paleozoic ocean existed between the SMM and SME.

Whereas Jian et al. (2012) reported ages of 354 Ma and 333 Ma of the microgabbro and plagiogranite from Xiaobaliang in the north of Hegenshan area (Fig. 1C) and suggested they represent an Alpine-type mantle diapir related with regional uplift after middle Paleozoic orogenic belt. Zhang et al. (2011) reported a typical bimodal high-K magmatic association with ages of 289–287 Ma in Bayinwula (Fig. 1C) ca. 60 km to the northwest of Sunid Zuoqi and suggested that it was developed under a post-collisional extensional regime. Based on 1:50000 geological mapping in the area 240 km to northeast of Hegenshan, Zhou et al. (2010b) reported a new discovery of the early-middle Permian cathaysian flora and suggested that the Paleo-Asian Ocean had closed before the early Permian. These data argue that the boundary between the SMM and SME is not characterized by a suture zone younger than ca. 350 Ma.

## 6. Tectonic evolution

According to new field investigation and geochronologic results, a tectonic evolutionary model of the CAOB in Inner Mongolia can be constructed as following (Fig. 17).

Before 500 Ma there was a block (HB) to the north of the northern margin of the NCC within the Paleo-Asian Ocean. On the northern and southern margins of the HB, the Ondor Sum Group was deposited, comprising clastic and volcanic rocks (Fig. 17A).

During 500–450 Ma time, the Paleo-Asian oceanic domains on the northern and southern sides of the HB subducted to the north beneath the SME and to the south beneath the northern continental margin of the NCC, respectively, building the north subduction system (NSS), characterized by arc diorites and granitoids, and the south subduction system (SSS), containing ophiolites and the Boin Sum Group arc volcanic rocks (Fig. 17B).

At 450–440 Ma, the ocean closure between the NCC and HB led to the collision of SSS with HB and formation of the SOB, including the mélange containing glaucophane and phengite with ages of 453.2 ± 1.8 Ma, 449.4 ± 1.8 Ma, and 445.6 ± 15 Ma in blueschists, and induced the deformation and metamorphism of the Ondor Sum Group in the northern SOB. Meanwhile, the northern subduction and NSS continued, forming arc diorite and granitoid belt extending from the Xilinhot to Airgin Sum areas (Fig. 17C).

During the 440–410 Ma time span, a retro-arc foreland basin formed on the southern side of the SOB, synchronously with the continuous uplift of the SOB magmatic arc, characterized by a wide distribution of the turbidite succession of the Xuniwusu Formation from the Tugurige to Boin Sum areas in the southern SOB, while the northward subduction still continued in the NSS (Fig. 17D).

During 410–380 Ma period, the HB, SMM and SME were amalgamated and the NOB formed, which is evidenced by the Upper Devonian mélange belt containing high pressure blueschists dated at 383 ± 13 Ma in the NOB and widespread development of the molasse basin in both the NOB and SOB, implying that an oceanic realm did not exist anymore between the NCC, HB, and SMM since the Late Devonian (Fig. 17E).

## 7. Conclusions

(1) Six tectonic units have been recognized in western Inner Mongolia, including, from south to north, the NCC, SOB, HB, NOB, SMM and SME, indicating that tectonic framework of

the CAOB in western Inner Mongolia is characterized by accretions of different blocks and building of orogenic belts;

(2) The SOB consists of four units, including, from north to south: fold belt, mélange, arc-pluton belt, and retro-arc foreland basin, representing a southern subduction–collision system between the NCC and HB blocks during the 500–440 Ma time. The NOB consists of four units: arc-pluton belt, mélange, foreland molasse basin, and fold belt, from north to south, representing a northern subduction–collision system between the HB and SMM blocks active during the 500–380 Ma time;

(3) A middle Paleozoic couple of convergent orogenic belts composed of the NOB and SOB constrained the consumption process of the Paleo-Asian Ocean in western Inner Mongolia during the early to middle Paleozoic, implying that oceanic lithosphere has not existed between the NCC, HB, and SMM since the Late Devonian. A double subduction–collision accretionary process, in the south and then in the north, is the dominant geodynamic feature for the eastern part of the CAOB during the early to middle Paleozoic.

## Acknowledgements

We thank Michel Faure for helpful discussion, Tong Qinlong, Li Ruibiao, Fang Junqing and Cheng Shengdong for their support in the field, Su Li for her help in ICP-MS analyses of zircons, and Wang Changqiu for his help in chemical analyses. We gratefully acknowledge constructive reviews from Xiao Wenjiao and two anonymous reviewers, as well as a careful editorial handling by guest-editor Zheng Yongfei. This study was supported by grants from the National Natural Science Foundation of China (40872145, 40821002) and the China geological survey projects (1212011220906). This is a contribution to IGCP#592 supported by UNESCO-IUGS.

## Appendix A.

## Analytical procedures for zircon samples

Zircons for ICP-MS analyses were separated from quartz diorites, sandstones and matrix of mélange according to magnetic properties and density and finally purified by hand picking. The zircons were cast in an epoxy mount and polished down to half section. Cathodoluminescence (CL) images were obtained for the zircons prior to analysis, using a CAMECA SX-50 microprobe at Peking University, in order to characterize internal textures and choose potential target sites for U–Pb dating. Laser ablation ICP-MS zircon U–Pb analyses were conducted on an Agilent 7500a ICP-MS equipped with a 193 nm laser in the China University of Geosciences Beijing. Laser spot size was set to ~ 36 μm for analyses, laser energy density at 8.5 J/cm2 and repetition rate at 10 Hz. The procedure of laser sampling is 5-s pre-ablation, 20-s sample chamber flushing and 40-s sampling ablation. The ablated material is carried into the ICP-MS by the high-purity Helium gas stream with flux of 0.8 L/min. The whole laser path was fluxed with N2 (15 L/min) and Ar (1.15 L/min) in order to increase energy stability. The counting time for U, Th, $^{204}$Pb, $^{206}$Pb, $^{207}$Pb and $^{208}$Pb is 20 ms. NIST SRM 610 silicate glass was external standard for concentration calculation and $^{29}$Si was internal standard (Pearce et al., 1997). U–Pb isotope fractionation effects were corrected using zircon 91500 (Wiedenbeck et al., 1995) as external standard. Zircon standard TEMORA (417 Ma) from Australia is also used as a secondary standard to supervise the deviation of age measurement/calculation (Black et al., 2004). Ten analyses for the standard

TEMORA yielded apparent $^{206}Pb/^{238}U$ ages of 408–420 Ma with a weighted mean of 415.7 ± 4.2 Ma (MSWD = 0.36). The detail analytical technique is described in Yuan et al. (2004). Isotopic ratios and element concentrations of zircons were calculated using GLITTER (ver. 4.4, Macquarie University). Concordia ages and diagrams were obtained using Isoplot/Ex (3.0, Ludwig, 2003). The common lead was corrected using LA-ICP-MS Common Lead Correction (ver. 3.15), followed the method of Andersen (2002). The mean ages are weighted means at 95% confidence levels (Ludwig, 2003). $^{206}Pb/^{238}U$ ages were used for samples younger than 1000 Ma, while $^{207}Pb/^{206}U$ ages were used for samples older than 1000 Ma.

## References


Andersen, 2002 T. Andersen Correction of common lead in U–Pb analyses that do not report $^{204}Pb$ Chemical Geology, 192 (2002), pp. 59–79

Badarch et al., 2002 G. Badarch, W.D. Gunningham, B.F. Windley A new terrane subdivision for Mongolia: implications for the Phanerozoic crustal growth of Central Asia Journal of Asian Earth Sciences, 21 (2002), pp. 87–110

Bayaraa et al., 2010 B. Bayaraa, N. Tsuchiya, G. Bignall Magmatism of the Shuteen complex and carboniferous subduction of the Gurvansaikhan terrane, South Mongolia Journal of Asian Earth Sciences, 37 (2010), pp. 399–411

Black et al., 2004 L.P. Black, S.L. Kamo, C.M. Allen, D.W. Davis, J.N. Aleinikoff, J.W. Valley, R. Mundil, I.H. Campbell, R.J. Korsch, I.S. Williams, C. Foudoulis Improved $^{206}Pb/^{238}U$ microprobe geochronology by the monitoring of a trace-element-related matrix effect; SHRIMP, ID-TIMS, ELA-ICP-MS and oxygen isotope documentation for a series of zircon standards Chemical Geology, 205 (2004), pp. 115–140

Blight et al., 2010 J.H.S. Blight, Q.G. Crowley, M.G. Petterson, D. Cunningham Granites of the Southern Mongolia carboniferous arc: new geochronological and geochemical constraints Lithos, 116 (2010), pp. 35–52

Buslovl et al., 2004 M.M. Buslovl, Y. Fujiwara, K. Iwata, N.N. Semakovl Late Paleozoic–Early Mesozoic geodynamics of Central Asia Gondwana Research, 7 (2004), pp. 791–808

Chen et al., 2000 B. Chen, B.M. Jahn, S. Wilde, B. Xu Two contrasting Paleozoic magmatic belts in northern Inner Mongolia, China: petrogenesis and tectonic implications Tectonophysics, 328 (2000), pp. 157–182

Chen et al., 2009 B. Chen, B.M. Jahn, W. Tian Evolution of the Solonker suture zone: constraints from zircon U–Pb ages, Hf isotopic ratios and whole-rock Nd–Sr isotope compositions of subduction- and collision-related magmas and forearc sediments Journal of Asian Earth Sciences, 34 (2009), pp. 245–257

Chen et al., 2012 C. Chen, Z.C. Zhang, Z.J. Guo Geochronology, geochemistry, and its geological significance of the Permian Mandula mafic rocks in Damaoqi, Inner Mongolia Science China Earth Sci, 55 (2012), pp. 39–52

Cope et al., 2005 T. Cope, B.D. Ritts, B.J. Darby, A. Fildani, S.A. Graham Late Paleozoic sedimentation on the Northern Margin of the North China Block: implications for

regional tectonics and climate change International Geology Review, 47 (2005), pp. 270–296

Darbya and Gehrels, 2006 B.J. Darbya, G. Gehrels Detrital zircon reference for the North China block Journal of Asian Earth Sciences, 26 (2006), pp. 637–648

De Jong et al., 2006 K. De Jong, W.J. Xiao, B.F. Windley, H. Masago, C.H. Lo Ordovician $^{40}Ar/^{39}Ar$ phengite ages from the blueschist-facies Ondor Sum subduction–accretion complex (Inner Mongolia) and implications for the Early Paleozoic history of continental blocks in China and adjacent areas American Journal of Science, 306 (2006), pp. 799–845

Demoux et al., 2009a A. Demoux, A. Kröner, G. Badarch, P. Jian, D. Tomurhuu, M.T.D. Wingate Zircon ages from the Baydrag Block and the Bayankhongor ophiolite zone: time constraints on late Neoproterozoic to Cambrian subduction- and accretion-related magmatism in Central Mongolia Journal of Geology, 117 (2009), pp. 377–397

Demoux et al., 2009b A. Demoux, A. Kröner, D. Liu, G. Badarch Precambrian crystalline basement in southern Mongolia as revealed by SHRIMP zircon dating International Journal of Earth Science, 98 (2009), pp. 1365–1380

Dickinson, 1974 W.R. Dickinson Plate tectonics and sedimentation Special Publication, SEPM, 22 (1974), pp. 1–27

Ge et al., 2011 M.C. Ge, W.X. Zhou, Y. Yu, J.J. Sun, J.Q. Bao, S.H. Wang Dissolution and supracrustal rocks dating of Xilin Gol Complex, Inner Mongolia, China Earth Science Frontiers, 18 (2011), pp. 182–195 (in Chinese with English abstract)

Geng et al., 2012 Y.S. Geng, L.L. Du, L.D. Ren Growth and reworking of the early Precambrian continental crust in the North China Craton: constraints from zircon Hf isotopes Gondwana Research, 21 (2012), pp. 517–529

Glorie et al., 2011 S. Glorie, J. De Grave, M.M. Buslov, F.I. Zhimulev, A. Izmer, W. Vandoorne, A. Ryabinin, P. Van den haute, F. Vanhaecke, M.A. Elburg Formation and Palaeozoic evolution of the Gorny–Altai–Altai-Mongolia suture zone (South Siberia): zircon U/Pb constraints on the igneous record Gondwana Research, 20 (2011), pp. 465–484

Gradstein et al., 2004 F.M. Gradstein, J.G. Ogg, A.G. Smith A Geologic Time Scale 2004 Cambridge University Press, Cambridge (2004) 610 pp.

Han et al., 1997 B.F. Han, S.G. Wang, B.M. Jahn, D.W. Hong, K. Hiroo, Y.L. Sun Depleted-mantle source for the Ulungur River A-type granites from North Xinjiang, China: geochemistry and Nd–Sr isotopic evidence, and implications for Phanerozoic crustal growth Chemical Geology, 138 (1997), pp. 135–159

Han et al., 2011 B.F. Han, G.Q. He, X.C. Wang, Z.J. Guo Late Carboniferous collision between the Tarim and Kazakhstan–Yili terranes in the western segment of the South Tian Shan Orogen, Central Asia, and implications for the North Xinjiang, western China Earth-Science Reviews, 109 (2011), pp. 74–93

Hanchar and Rundnick, 1995 J.M. Hanchar, R.L. Rundnick Revealing hidden structures: the application of cathodoluminescence and back-scattered electron imaging to dating zircons from lower crustal xenoliths Lithos, 36 (1995), pp. 289–303

Hong et al., 1996 D.W. Hong, S.G. Wang, B.F. Han, M.Y. Jin Post-orogenic alkaline granites from China and comparisons with anorogenic alkaline granites elsewhere Journal of Southeast Asian Earth Sciences, 13 (1996), pp. 13–27

Hong et al., 2004 D.W. Hong, J.S. Zhang, T. Wang, S.G. Wang, X.L. Xie Continental crustal growth and the supercontinental cycle: evidence from the Central Asian Orogenic Belt Journal of Asian Earth Sciences, 23 (2004), pp. 799–813

Hsü et al., 1991 K.J. Hsü, Q. Wang, J. Li, J. Hao Geologic evolution of the Neimonides: a working hypothesis Eclogae Geologicae Helvetiae, 84 (1991), pp. 1–31

Hu et al., 1990 X. Hu, C. Xu, S. Niu Evolution of the Early Paleozoic Continental Margin in Northern Margin of the North China Platform Peking University Press, Beijing (1990) 215 pp. (in Chinese with English abstract)

IMBGMR (Inner Mongolian Bureau of Geology and Mineral Resources), 1991 IMBGMR (Inner Mongolian Bureau of Geology and Mineral Resources) Regional Geology of Inner Mongolian Autonomous Region Geological Publishing House, Beijing (1991) 726 pp. (in Chinese with English abstract)

Jahn et al., 2000a B.M. Jahn, F.Y. Wu, B. Chen Granitoids of the Central Asian Orogenic Belt and continental growth in the Phanerozoic Transactions of the Royal Society of Edinburgh: Earth Sciences, 91 (2000), pp. 181–193

Jahn et al., 2000b B.M. Jahn, F.Y. Wu, B. Chen Massive granitoid generation in Central Asia: Nd isotope evidence and implication for continental growth in the Phanerozoic Episodes, 23 (2000), pp. 82–92

Jahn et al., 2009 B.M. Jahn, B.A. Litvinovsky, A.N. Zanvilevich, M. Reichow Peralkaline granitoid magmatism in the Mongolian–Transbaikalian Belt: evolution, petrogenesis and tectonic significance Lithos, 113 (2009), pp. 521–539

Jian et al., 2008 P. Jian, D. Liu, A. Kröner, B.F. Windley, Y. Shi, F. Zhanf, G. Shi, L. Miao, W. Zhang, Q. Zhang, L. Zhang, J. Ren Time scale of an early to mid-Paleozoic orogenic cycle of the long-lived Central Asian Orogenic Belt, Inner Mongolia of China: implications for continental growth Lithos, 101 (2008), pp. 233–259

Jian et al., 2010 P. Jian, D. Liu, A. Kröner Evolution of a Permian intraoceanic arc-trench system in the Solonker suture zone, Central Asian Orogenic Belt, China and Mongolia Lithos, 118 (2010), pp. 169–190

Jian et al., 2012 P. Jian, A. Kröner, B.F. Windley, Y. Shi, W. Zhang, L. Zhang, W. Yang Carboniferous and Cretaceous mafic–ultramafic massifs in Inner Mongolia (China): A SHRIMP zircon and geochemical study of the previously presumed integral“Hegenshan ophiolite” Lithos, 142–143 (2012), pp. 48–66

Khain et al., 2002 E.V. Khain, E.V. Bibikova, A. Kröner, D.Z. Zhuravlev, E.V. Sklyarov, A.A. Fedotova, I.R. Kravchenko-Berezhnoy The most ancient ophiolite of the Central Asian fold belt: U–Pb and Pb–Pb zircon ages for the Dunzhugur Complex, Eastern Sayan, Siberia, and geodynamic implications Earth and Planetary Science Letters, 199 (2002), pp. 311–325

Khain et al., 2003 E.V. Khain, E.V. Bibikova, E.B. Salnikova, A. Kröner, A.S. Gibsher, A.N. Didenko, K.E. Degtyarev, A.A. Fedotova The Palaeo-Asian Ocean in the Neoproterozoic and early Palaeozoic: new geochronologic data and palaeotectonic reconstructions Precambrian Research, 122 (2003), pp. 329–358

Kröner et al., 2007 A. Kröner, B.F. Windley, G. Badarch Accretionary growth and crust-formation in the Central Asian Orogenic Belt and comparison with the Arabian–Nubian shield Geological Society of America Memoir, 200 (2007), pp. 181–209

Kröner et al., 2010 A. Kröner, J. Lehmann, K. Schulmann, A. Demoux, O. Lexa, D. Tomurhuu, P. Stipska, D. Liu, M. Wingate Lithostratigraphic and geochronological constrains on the evolution of the Central Asian orogenic belt in SW Mongolia: Early Paleozoic rifting followed by Late Paleozoic accretion American Journal of Science, 310 (2010), pp. 523–574

Kröner et al., 2011 A. Kröner, A. Demoux, T. Zack, Y. Rojas-Agramonte, P. Jian, D. Tomurhuu, M. Barth Zircon ages for a felsic volcanic rock and arc-related early Palaeozoic sediments on the margin of the Baydrag microcontinent, central Asian orogenic belt, Mongolia Journal of Asian Earth Sciences, 42 (2011), pp. 1008–1017

Li, 2006 J.Y. Li Permian geodynamic setting of Northeast China and adjacent regions: closure of the Paleo-Asian Ocean and subduction of the Paleo-Pacific Plate Journal of Asian Earth Sciences, 26 (2006), pp. 207–224

Li et al., 2010a J.F. Li, Z.C. Zhang, B.F. Han Ar–Ar and zircon SHRIMP geochronology of hornblendite and diorite in northern Darhan Muminggan Joint Banner, Inner Mongolia, and its geological significance Acta Petrologica et Mineralogica, 29 (2010), pp. 732–740 (in Chinese with English abstract)

Li et al., 2010b Y.L. Li, H.W. Zhou, F.M. Brouwer, J.R. Wijbrans, Z.Q. Zhong, H.F. Liu Tectonic significance of the Xilin Gol Complex, Inner Mongolia, China: petrological, geochemical and U–Pb zircon age constraints Journal of Asian Earth Sciences, 42 (2010), pp. 1018–1029

Li et al., 2011 D.P. Li, Y.L. Chen, Z. Wang, K.J. Houand, C.Z. Liu Detrital zircon U_Pb ages, Hf isotopes and tectonic implications for Palaeozoic sedimentary rocks from the Xing-Meng Orogenic Belt, Middle-East Part of Inner Mongolia, China Geological Journal, 46 (2011), pp. 63–81

Liu et al., 2003 D. Liu, P. Jian, Q. Zhang, F. Zhanf, Y. Shi, G. Shi, L. Zhang, H. Tao SHRIMP dating of adakites in the Tulingkai ophiolite, Inner Mongolia: evidence for the Eraly Paleozoic subduction Acta Geologica Sinica, 77 (2003), pp. 317–326

Ludwig, 2003 K.R. Ludwig User's manual for Isoplot 3.0: a geochronological toolkit for Microsoft Excel Berkeley Geochronology Center Special Publication, 4 (2003) 71 pp.

Miao et al., 2007 L. Miao, F. Zhang, W. Fan, D. Liu Phanerozoic evolution of the Inner Mongolia Daxinganling orogenic belt in North China: constraints from geochronology of ophiolites and associated formations Geological Society London, Special Publications, 280 (2007), pp. 223–237

Mossakovsky et al., 1993 A.A. Mossakovsky, S.V. Ruzhentsev, S.G. Samygin, T.N. Kheraskova Central Asian fold belt: geodynamic evolution and history of formation Geotectonics, 6 (1993), pp. 3–33

Pearce, 1984 J.A. Pearce Trace element discrimination diagrams for the tectonic interpretation of granitic rocks Journal of Petrology, 25 (1984), pp. 956–983

Pearce et al., 1997 N.J.G. Pearce, W.T. Perkins, J.A. Westgate, M.P. Gorton, S.E. Jackson, C.R. Neal, S.P. Chenery A compilation of new and published major and trace element data for NIST SRM 610 and NIST SRM 612 glass reference materials Geostandards Newsletter, 21 (1997), pp. 115–141

Robinson et al., 1999 P.T. Robinson, M.F. Zhou, X.F. Hu, P. Reynolds, W.J. Bai, J. Yang Geochemical constraints on the origin of the Hegenshan ophiolite, Inner Mongolia, China Journal of Asian Earth Sciences, 17 (1999), pp. 423–442

Rojas-Agramonte et al., 2011 Y. Rojas-Agramonte, A. Kröner, A. Demoux, X. Xia, W. Wang, T. Donskaya, D. Liu, M. Sun Detrital and xenocrystic zircon ages from eoproterozoic to Palaeozoic arc terranes of Mongolia: significance for the origin of crustal fragments in the Central Asian Orogenic Belt Gondwana Research, 19 (2011), pp. 751–763

Safonova et al., 2004 I.Y. Safonova, M.M. Buslov, K. Iwata, D.A. Kokh Fragments of Vendia—early Carboniferous oceanic crust of the Paleo-Asian Ocean in foldbelts of the Altai-Sayan region of Central Asia: geochemistry, biostratigraphy and structural setting Gondwana Research, 7 (2004), pp. 771–790

Sengör and Natal'in, 1996 A.M.C. Sengör, B.A. Natal'in Paleotectonics of Asia: fragments of a synthesis A. Yin, T.M. Harrison (Eds.), The Tectonic Evolution of Asia, Cambridge University Press, Cambridge (1996), pp. 486–641

Sengör et al., 1993 A.M.C. Sengör, B.A. Natal'in, V.S. Burtman Evolution of the Altaid tectonic collage and Palaeozoic crustal growth in Eurasia Nature, 364 (1993), pp. 299–307

Shao, 1986 J.A. Shao Early Paleozoic ophiolite in middle Inner Mongolia and its implications for reconstruct crust evolution Collection of Papers on Tectonics of North China Plate, Earthquake Publishing House, Beijing (1986), pp. 87–101 (in Chinese)

Shao, 1991 J.A. Shao Crust Evolution in the Middle Part of the Northern Margin of Sino-Korean Plate Peking University Press, Beijing (1991) 136 pp. (in Chinese with English abstract)

Shi et al., 2003 G.H. Shi, D.Y. Liu, F.Q. Zhang, P. Jiang, L.C. Miao, Y.R. Shi, H. Tao SHRIMP U–Pb zircon geochronology and its implications on the Xilin Gol Complex, Inner Mongolia, China Chinese Science Bulletin, 48 (2003), pp. 2742–2748

Shi et al., 2004a G.H. Shi, L.C. Miao, F.Q. Zhang, P. Jian, W.M. Fan, D.Y. Liu The age and its regional tectonic implication of the Xilinhot A-type granites, Inner Mongolia Chinese Science Bulletin, 49 (2004), pp. 384–389

Shi et al., 2004b Y.R. Shi, D.Y. Liu, Q. Zhang, F.Q. Zhang, L.C. Miao, G.H. Shi, L.Q. Zhang, H. Tao SHRIMP dating of diorites and granites in Southern Suzuoqi, InnerMongolia Acta Geologica Sinica, 78 (2004), pp. 789–799 (in Chinese with English abstract)

Shi et al., 2005 Y.R. Shi, D.Y. Liu, Q. Zhang, P. Jiang, F.Q. Zhang, L.C. Miao, Y.R. Shi, H. Tao The petrogenesis and SHRIMP dating of the Baiyinbaolidao adakitic rocks in southern Suzuoqi, Inner Mongolia Acta Petrologica Sinica, 21 (2005), pp. 143–150 (in Chinese with English abstract)

Stipska et al., 2010 P. Stipska, K. Schulmann, J. Lehmann, M. Corsini, O. Lexa, D. Tomurhuu Early Cambrian eclogites in SW Mongolia: evidence that the Palaeo-Asian Ocean suture extends further east than expected Journal of Metamorphic Geology (2010) http://dx.doi.org/10.1111/j.1525-1314.2010.00899.x

Sun and McDonough, 1989 S.S. Sun, W.F. McDonough Chemical and isotopic systematics of ocean basalts: implications for mantle composition and processes ,in: A.D. Saunders, M.J. Norry (Eds.), Magmatism in the Ocean Basins, Geological Society Special Publications, 42 (1989), pp. 313–345

Tang, 1990 K.D. Tang Tectonic development of Paleozoic fold belts at the north margin of the Sino–Korean craton Tectonics, 9 (1990), pp. 249–260

Tang, 1992 K.D. Tang Tectonic evolution and minerogenetic regularities of the fold belt along the Northern Margins of Sino-Korean Plate Peking University Press, Beijing (1992) 277 pp. (in Chinese with English abstract)

Tang and Zhang, 1991 K.D. Tang, Y.P. Zhang Tectonic evolution of Inner Mongolia X.C. Xiao, Y.Q. Tang (Eds.)Scientific and Tectonical Publishing House, Beijing (1991), pp. 30–53 (in Chinese with English abstract)

Tang et al., 2011 W.H. Tang, Z.C. Zhang, J.F. Li, Z.S. Feng, C. Chen Geochemistry of the Carboniferous volcanic rocks of Benbatu Formation in Sonid Youqi, Inner Mongolia and its geological significance Acta Scientiarum Naturalium Universitatis Pekinensis, 47 (2011), pp. 321–330

Walker, 1979 R.G. Walker Deep water sandstone facies and ancient submarine fans: models for exploration for stratigraphic traps American Association of Petroleum Geologists Bulletin, 62 (1979), pp. 932–966

Wan et al., 2011 Y.S. Wan, D.Y. Liu, W. Wang, T.R. Song, A. Kröner, C.Y. Dong, H.Y. Zhou, X.Y. Yin Provenance of meso- to neoproterozoic cover sediments at the Ming Tombs, Beijing, North China Craton: an integrated study of U–Pb dating and Hf isotopic measurement of detrital zircons and whole-rock geochemistry Gondwana Research, 20 (2011), pp. 219–242

Wang et al., 2001 T. Wang, Y.D. Zheng, G.E. Gehrels, Z.G. Mu Geochronological evidence for existence of South Mongolian microcontinent-A zircon UPb age of granitoid gneisses

from the Yagan-Onch Hayrhan metamorphic core complex Chinese Science Bulletin, 46 (2001), pp. 2005–2008

Wiedenbeck et al., 1995 M. Wiedenbeck, P. Alle, F. Corfu, W.L. Griffin, M. Meier, F. Oberli, A. Vonquadt, J.C. Roddick, W. Speigel Three natural zircon standards for U–Th–Pb, Lu–Hf, trace-element and REE analyses Geostandards Newsletter, 19 (1995), pp. 1–23

Wilde et al., 2002 S.A. Wilde, G.C. Zhao, M. Sun Development of the North China Craton during the Late Archaean and its final amalgamation at 1.8 Ga; some speculations on its position within a global Palaeoproterozoic Supercontinent Gondwana Research, 5 (2002), pp. 85–94

Windley et al., 2007 B.F. Windley, D. Alexeiev, W.J. Xiao, A. Kröner, G. Badarch Tectonic models for accretion of the Central Asian Orogenic Belt Journal of the Geological Society of London, 164 (2007), pp. 31–47

Xiao et al., 2003 W.J. Xiao, B. Windley, J. Hao, M.G. Zhai Accretion leading to collision and the Permian Solonker suture, Inner Mongolia, China: termination of the Central Asian Orogenic Belt Tectonics, 22 (2003), pp. 1069–1089
http://dx.doi.org/10.1029/2002TC001484

Xiao et al., 2004 W.J. Xiao, B.F. Windley, G. Badarch, S. Sun, J. Li, K. Qin, Z. Wang Palaeozoic accretionary and convergent tectonics of the southern Altaids: implications for the growth of Central Asia Journal of the Geological Society of London, 161 (2004), pp. 339–342

Xiao et al., 2009 W. Xiao, B.F. Windley, B.C. Huang, C.M. Han, C. Yuan, H.L. Chen, M. Sun, S. Sun, J.L. Li End-Permian to mid-Triassic termination of the accretionary processes of the southern Altaids: implications for the geodynamic evolution, Phanerozoic continental growth, and metallogeny of Central Asia International Journal of Earth Science, 98 (2009), pp. 1189–1287

Xiao et al., 2010 W.J. Xiao, J. Mao, B.F. Windley, C.M. Han, J.F. Qu, J.E. Zhang, S.J. Ao, Q.Q. Guo, N.R. Cleven, S.F. Lin, Y.H. Shan, J.L. Li Paleozoic multiple accretionary and collisional processes of the Beishan orogenic collage American Journal of Science, 310 (2010), pp. 1553–1594

Xu and Charvet, 2010 B. Xu, J. Charvet Mid-Paleozoic opposite Orogenic Belt in Inner Mongolia of China and its significance for Central Asian Orogenic Belt International Association for Gondwana Research Conference Series 9, Qingdao, China, Abstract Volume (2010), p. 84

Xu and Chen, 1993 B. Xu, B. Chen The opposite subduction and collision between the Siberian and Sino-Korean plates during the early-middle Paleozoic Report No: 4 of the IGCP Projrct 283: Geodynamic Evolution of Paleoasian Ocean, Novosibirsk, USSR (1993), pp. 148–150

Xu and Chen, 1997 B. Xu, B. Chen Framework and evolution of the middle Paleozoic orogenic belt between Siberian and North China Plates in northern Inner Mongolia Science in China. Series D, 40 (1997), pp. 463–469

Xu et al., 1994 Xu, B., Chen, B., Bai, Z., Zhang, C., 1994. Geological map (1:50,000) and geologic report of Baiyanbaolidao area, Inner Mongolia. Peking University.

Xu et al., 2000 B. Xu, S.W. Liu, C.Q. Wang, H.F. Zheng, F. Tian Sm–Nd, Rb–Sr Geochronology of the Baoyintu Group in Northwestern Inner Mongolia Geological Review, 46 (2000), pp. 86–90

Xu et al., 2001a B. Xu, J. Charvet, F.Q. Zhang Primary study on petrology and geochronology of the blueschist in Sonid Zuoqi, northern Inner Mongolia Chinese Journal of Geology, 36 (2001), pp. 424–434 (in Chinese with English abstract)

Xu et al., 2001b Xu, B., Liu, S.W., Wang C.Q., Zheng, H.F., 2001b. Geological map (1:50,000) and geologic report of Tugurige area, Inner Mongolia. Peking University.

Xu et al., 2003 L.Q. Xu, J.F. Deng, Z.Y. Chen, J.X. Tao The identification of Ordovician adakites and its signification in northern Damao, Inner Mongolia Geoscience, 17 (2003), pp. 428–434 (in Chinese with English abstract)

Xue et al., 2009 H.M. Xue, L.J. Guo, Z.Q. Hou, X.W. Zhou, Y. Tong, X.F. Pan The Xilingele complex from the eastern part of the Central Asian-Mongolia Orogenic Belt, China: products of Early Variscan orogeny other than ancient block: Evidence from zircon SHRIMP U–Pb ages Acta Petrologica Sinica, 25 (2009), pp. 2001–2010

Yang et al., 2006 J.H. Yang, F.Y. Wu, J.A. Shao, S.A. Wilde, L.W. Xie, X.M. Liu Constraints on the timing of uplift of the Yanshan Fold and Thrust Belt, North China Earth and Planetary Science Letters, 246 (2006), pp. 336–352

Yarmolyuk et al., 2005 V.V. Yarmolyuk, V.I. Kovalenko, E.B. Sal'nikova, I.K. Kozakov, A.B. Kotov, V.P. Kovach, N.V. Vladykin, S.Z. Yakovleva U–Pb age of syn- and postmetamorphic granitoids of South Mongolia: evidence for the presence of Grenvillides in the Central Asian Foldbelt Doklady Earth Sciences, 404 (2005), pp. 986–990

Yarmolyuk et al., 2008 V.V. Yarmolyuk, V.I. Kovalenko, E.B. Sal'nikova, V.P. Kovach, A.M. Kozlovsky, A.B. Kotov, V.I. Lebedev Geochronology, igneous rocks and formation of the Late Paleozoic South Mongolian Active Margin of the Siberian Continent Stratigraphy and Geological Correlation, 2 (2008), pp. 162–181

Yuan et al., 2004 H.L. Yuan, S. Gao, X.M. Liu, H.M. Li, D. Günther, F.Y. Wu Accurate U–Pb age and trace element determinations of zircon by laser ablation inductively coupled plasma-mass spectrometry Geostandards and Geoanalytical Research, 28 (2004), pp. 353–370

Zeng, 1990 Q.D. Zeng The features of the ductile shear deformation of the early Paleozoic Boin Sum group in the middle part of the Inner Mongolia Jilin Geology, 2 (1990), pp. 65–72 (in Chinese with English abstract)

Zhai and Santosh, 2011 M.G. Zhai, M. Santosh The early Precambrian odyssey of the North China Craton: a synoptic overview Gondwana Research, 20 (2011), pp. 6–25

Zhang, 2010 Zhang, W., 2010. SHRIMP dating of the early Paleozoic Bainaimiao Arc and Permian granitoids on the northern margin of North China craton, Inner Mongolia, Doctoral Dissertation (in Chinese with English abstract).

Zhang and Jian, 2008 W. Zhang, P. Jian SHRIMP dating of Early Paleozoic granites from north Damaoqi, Inner Mongolia Acta Geologica Sinica, 82 (2008), pp. 778–787 (in Chinese with English abstract)

Zhang and Tang, 1989 Y.P. Zhang, K.D. Tang Pre-Jurassic tectonic evolution of intercontinental region and the suture zone between the North China and Siberian platforms Journal of Southeast Asian Earth Sciences, 3 (1989), pp. 47–55

Zhang et al., 2004 J.F. Zhang, Q.B. Pang, Q. Zhu, C.Z. Jin, G.J. Liu Zircon U–Pb dating of the Bayan Bold granite-porphyry in Inner Mongolia: the age of the host rock of the Bayan Bold gold deposit Regional Geology of China, 23 (2004), pp. 189–192 (in Chinese with English abstract)

Zhang et al., 2007 S.H. Zhang, Y. Zhao, B. Song, Z.Y. Yang, J.M. Hu, H. Wu Carboniferous granitic plutons from the northern margin of the North China block: implications for a late Palaeozoic active continental margin Journal of the Geological Society of London, 164 (2007), pp. 451–463

Zhang et al., 2009a S.H. Zhang, Y. Zhao, B. Song, J.M. Hu, S.W. Liu, Y.H. Yang, F.K. Chen, X.M. Liu, J. Liu Contrasting late Carboniferous and late Permian-middle Triassic intrusive suites from the northern margin of the north China craton Geological Society of America Bulletin, 121 (2009), pp. 181–200

Zhang et al., 2009b S.H. Zhang, Y. Zhao, Z.Y. Yang, Z.F. He, H. Wu The 1.35 Ga diabase sills from the northern North China Craton: implications for breakup of the Columbia (Nuna) supercontinent Earth and Planetary Science Letters, 288 (2009), pp. 588–600

Zhang et al., 2010 Y.P. Zhang, Y.Z. Su, J.C. Li Regional tectonic significance of the Late Silurian Xibiehe Formation in central Inner Mongolia, China Geological Bulletin of China, 29 (2010), pp. 1599–1605 (in Chinese with English abstract)

Zhang et al., 2011 X.H. Zhang, S.A. Wilde, H.F. Zhang, M.G. Zhai Early Permian high-K calc-alkaline volcanic rocks from NW Inner Mongolia, North China: geochemistry, origin and tectonic implications Journal of the Geological Society of London, 168 (2011), pp. 525–543

Zhao et al., 2001 G.C. Zhao, S.A. Wilde, P.A. Cawood, M. Sun, L.Z. Lu Archean blocks and their boundaries in the North China Craton: lithological, geochemical, structural and P–T path constraints Precambrian Research, 107 (2001), pp. 45–73

Zhao et al., 2002 G.C. Zhao, P.A. Cawood, S.A. Wilde, M. Sun Review of global2.1–1.8 Ga orogens: implications for a pre-Rodinia supercontinent Earth-Science Reviews, 59 (2002), pp. 125–162

Zhou et al., 2009 J.B. Zhou, S.A. Wilde, X.Z. Zhang, G.C. Zhao, C.Q. Zheng, Y.J. Wang, X.H. Zhang The onset of Pacific margin accretion in NE China: evidence from the Heilongjiang high-pressure metamorphic belt Tectonophysics, 2009 (2009), pp. 230–246

Zhou et al., 2010a J.B. Zhou, S.A. Wilde, G.C. Zhao, X.Z. Zhang, H. Wang, W.S. Zeng Was the easternmost segment of the Central Asian Orogenic Belt derived from Gondwana or Siberia: an intriguing dilemma? Journal of Geodynamics, 50 (2010), pp. 300–317

Zhou et al., 2010b Z.G. Zhou, Y.C. Gu, C.F. Liu, Y.S. Yu, B. Zhang, Z.J. Tian, F.B. He, B.R. Wang Discovery of Early–Middle Permian cathaysian flora in Manduhubaolage area, Dong Ujimqin Qi, Inner Mongolia, China and its geological significance Geological Bulletin of China, 29 (2010), pp. 21–25 (in Chinese with English abstract)

Zhou et al., 2011 J.B. Zhou, S.A. Wilde, X.Z. Zhang, G.C. Zhao, F.L. Liu, D.W. Qiao, S.M. Ren, J.H. Liu A>1300 km late Pan-African metamorphic belt in NE China: new evidence from the Xing'an block and its tectonic implications Tectonophysics, 509 (2011), pp. 280–292

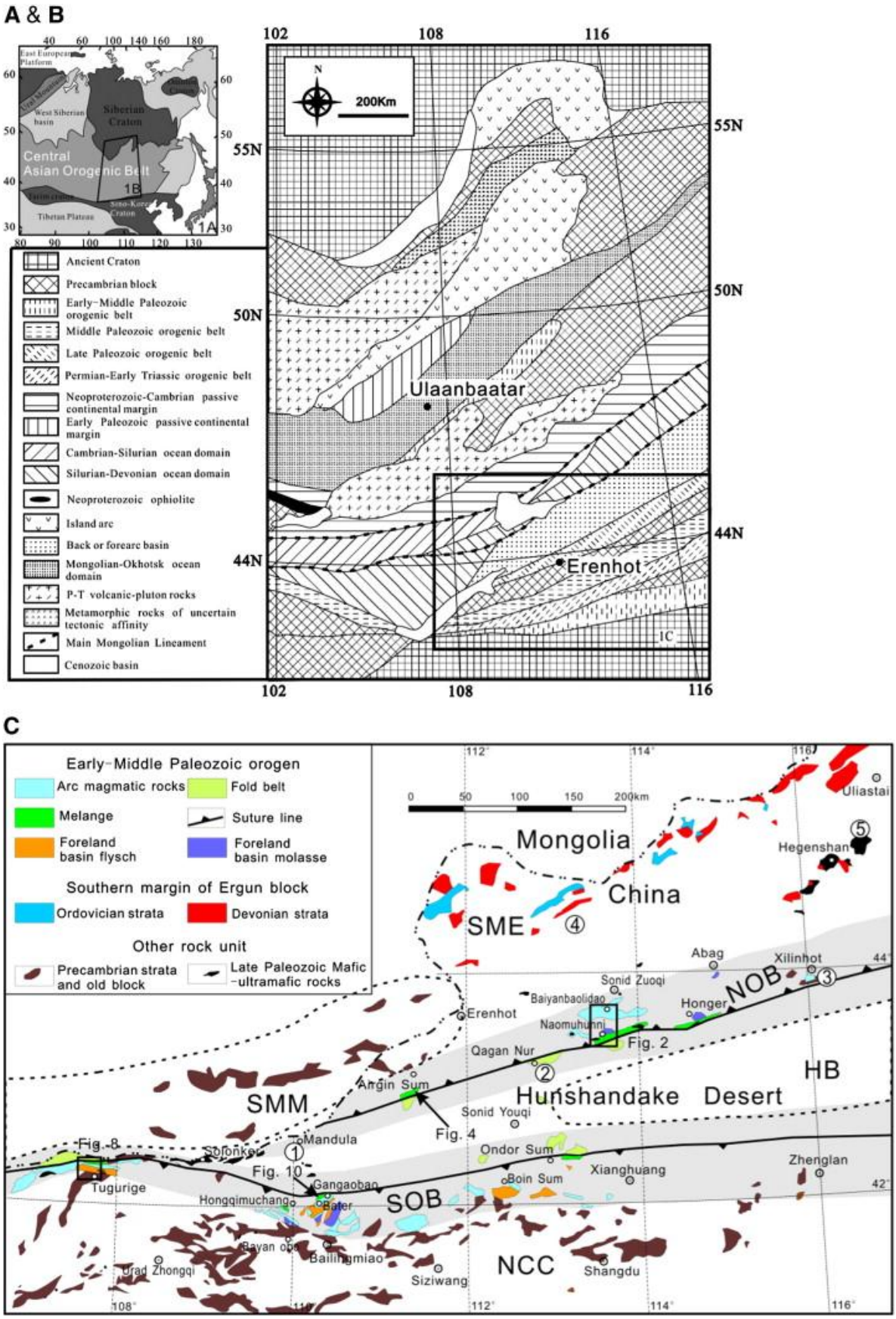


Fig. 1. (A) Location of the Central Asian Orogenic Belt (CAOB). (B) Sketch geologic map of units between the Siberia and North China Cratons (compiled from [Badarch et al., 2002], [Xiao et al.,

2003], [Kröner et al., 2010] and [Stipska et al., 2010]). (C). Tectonic map of western Inner Mongolia emphasizing the Early and Middle Paleozoic outcrops and Precambrian blocks (compiled from [Shao, 1991], IMBGMR (Inner Mongolian Bureau of Geology and Mineral Resources), 1991, [Xiao et al., 2003], [Jian et al., 2008] and [Yarmolyuk et al., 2008]). ①–⑤ mark the Late Paleozoic magmatic rocks that are discussed in Section 5.3; ① Permian mafic rocks of 279–274 Ma (Chen et al., 2012); ② Bimodal volcanic suite of 313–308 Ma (Tang et al., 2011); ③ A-type granite of 276 Ma ( [Shi et al., 2004a] and [Shi et al., 2004b]); ④ Mafic and felsic volcanic rocks of 289–287 Ma (Zhang et al., 2011); ⑤ Hegenshan mafic-ultramafic rocks of 354–333 Ma (Jian et al., 2012) and ca.295 Ma (Miao et al., 2007). The positions of Fig. 2, Fig. 4, Fig. 8 and Fig. 10 are marked.

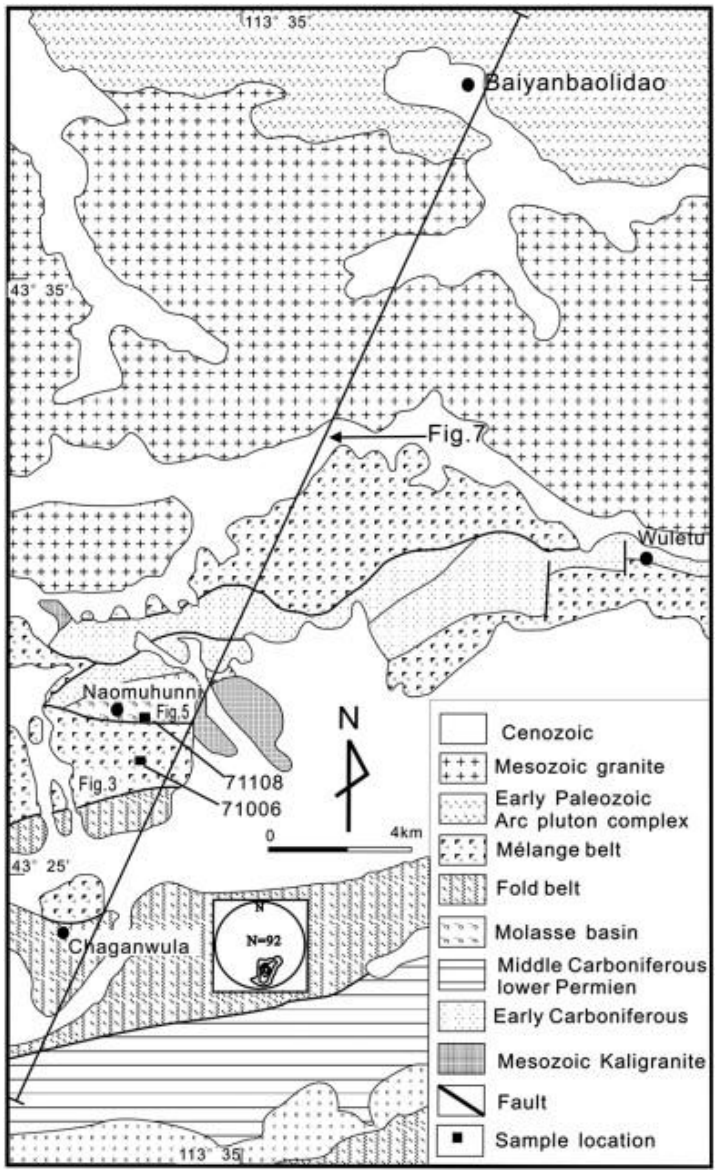


Fig. 2. Geological map showing the tectonic units of the NOB in Baiyanbaolidao area (after Xu et al., 1994). The section line of Fig. 7, locations of Fig. 3 and Fig. 5 are marked (see Fig. 1C for location of Fig. 2). The inset shows equal-area, lower-hemisphere stereoplots of the axial-plane foliations in the fold belt.

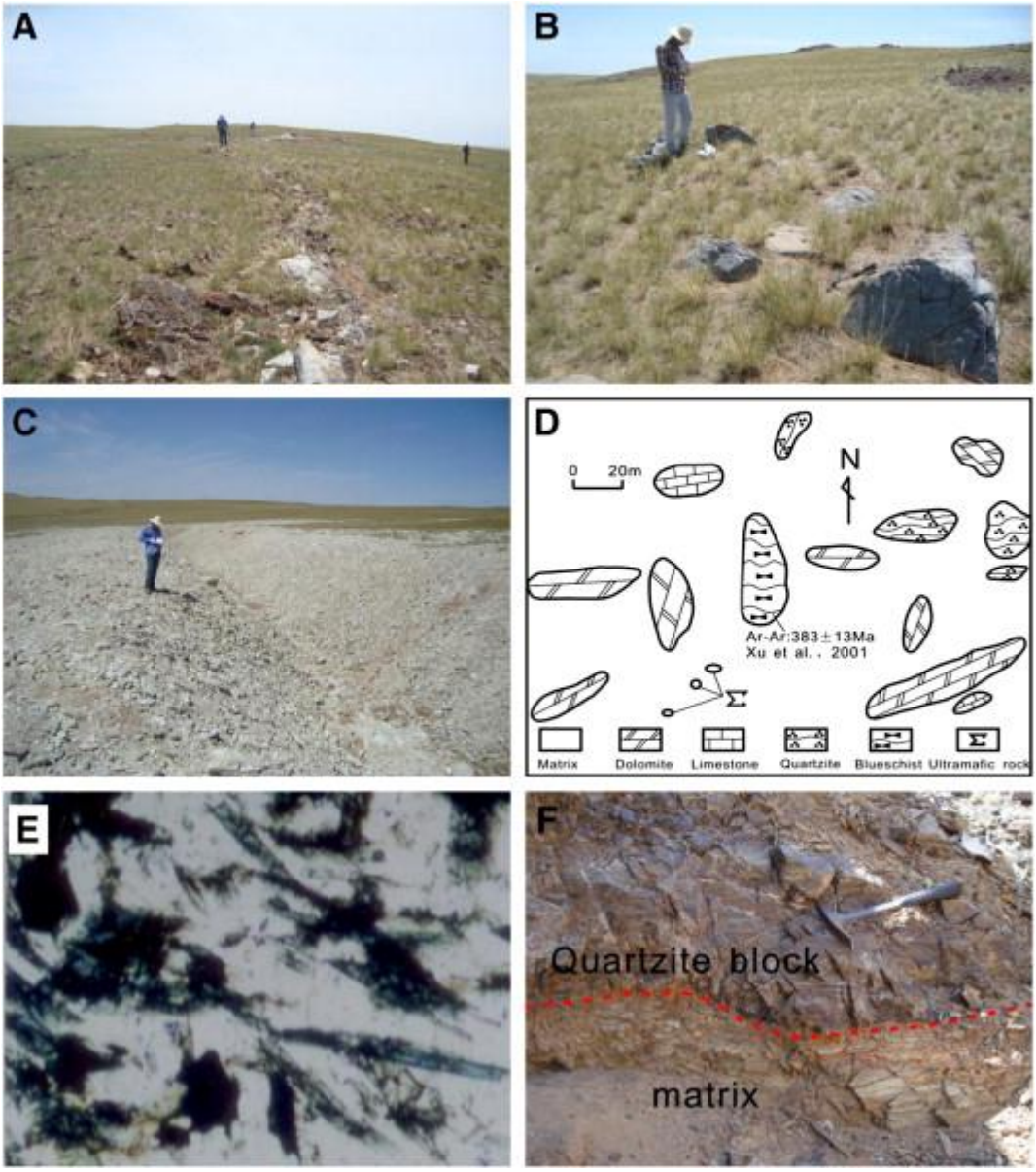


Fig. 3. Photographs and sketch of typical outcrop of mélange near Naomuhunni (see Fig. 2 for location). A: dolomite block; B: limestone block; C: ultramafic block; D: distribution of blocks near Naomuhunni; E: Photomicrograph of Na-amphibole in blueschist block; F: fault relationship between matrix and quartzite block (red line).


Fig. 4. Photographs of the mélange belt in the Airgin Sum area. A: gentle relief and isolated blocks; B: foliated dolomite block; C: foliated mafic rock block; D: foliated granite block (see Fig. 1C for location).

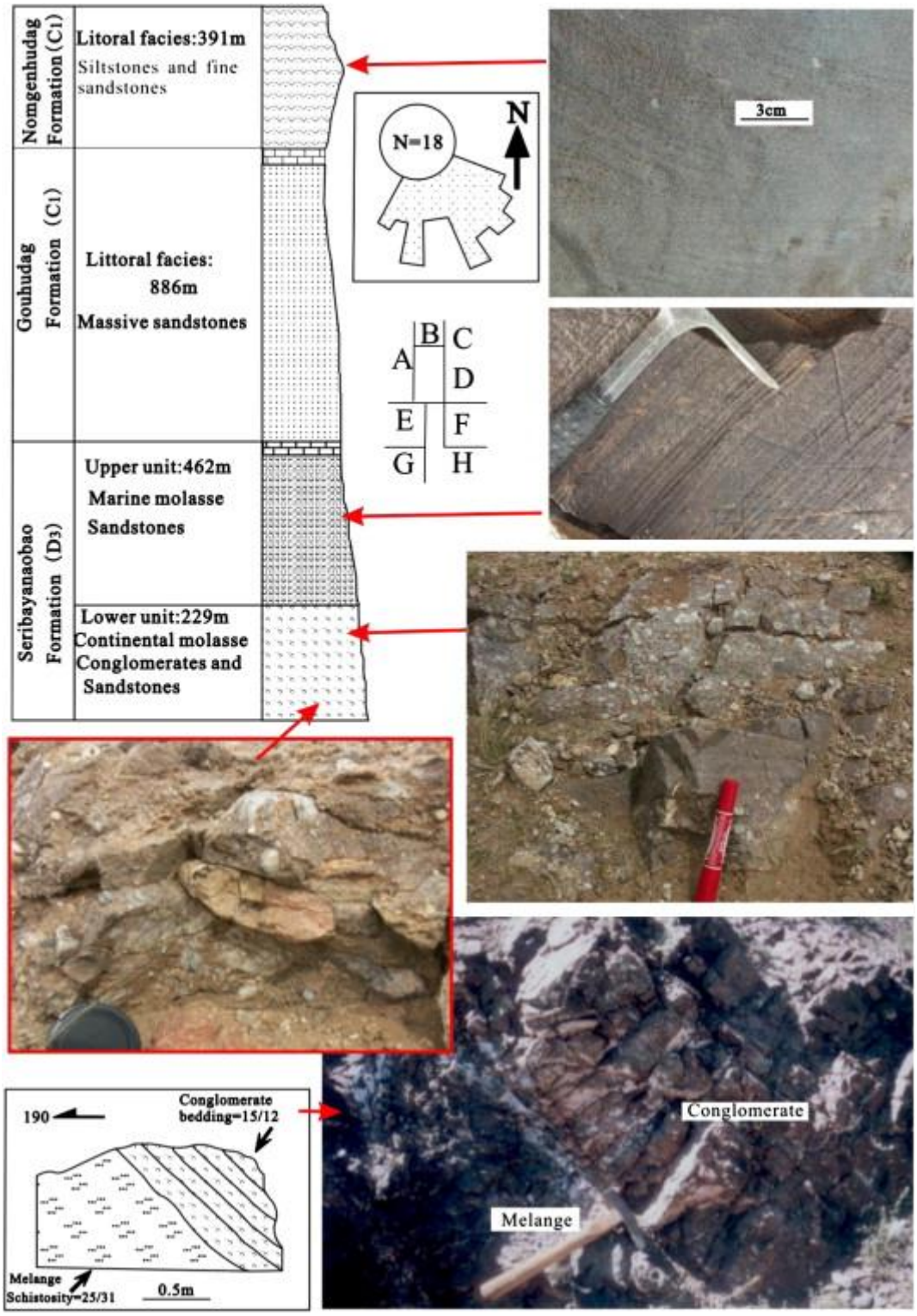


Fig. 5. Stratigraphic sequence and photographs of the molasse basin in Naomuhunni. (see Fig. 2 for location). A: Upper Devonian and Lower Carboniferous column; B: paleocurrent trend; C: small inclined bedding in sandstone; D: flat bedding in sandstone; E: gravels in red conglomerate; F: red thick conglomerate; G: interpretative redrawing of H; H: angular unconformity between the Upper Devonian conglomerate and the underlying mélange.

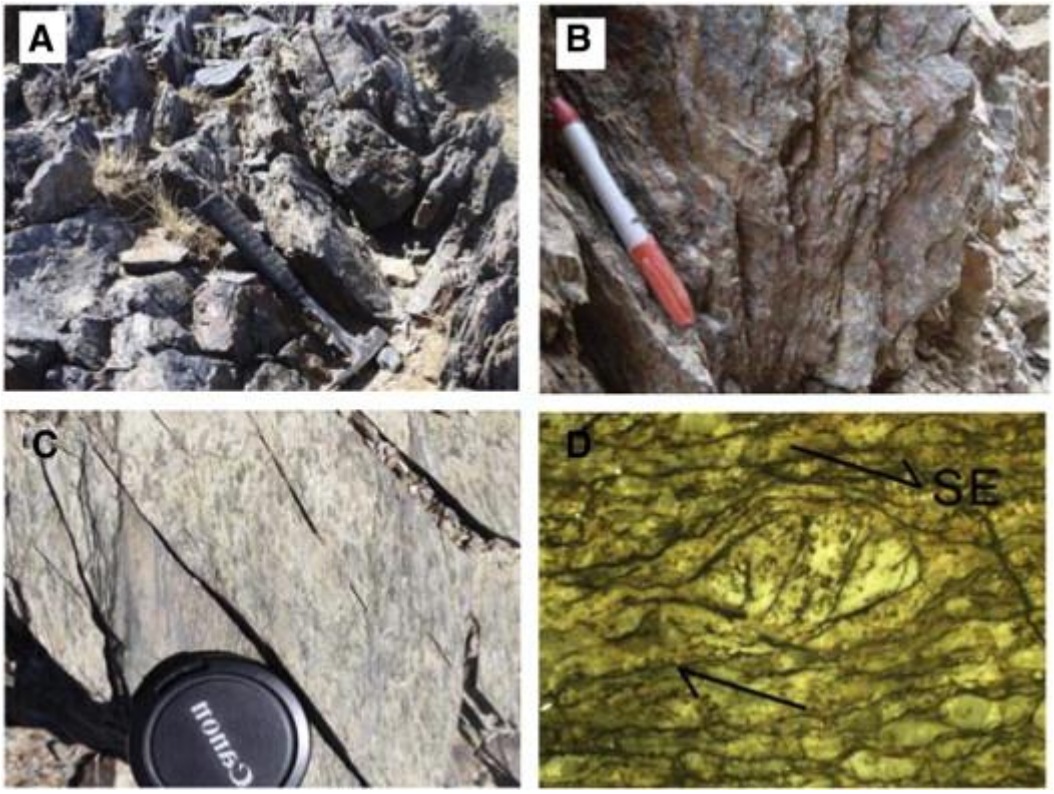


Fig. 6. Representative field deformation features in the NOB. A: south-verging slightly inverted fold in the Ondor Sum Group, Baiyanbaolidao; B: penetrative axial-plane foliations in the Ondor Sum Group, Baiyanbaolidao; C: northwest-dipping foliations and top-to-southeast lineations made of biotites in the granitic ductile shear belt, Airgin Sum; D: ribbons of recrystallized quartz and fragmented feldspar, showing asymmetric pressure shadows with a top-to-the-SE sense of shearing.

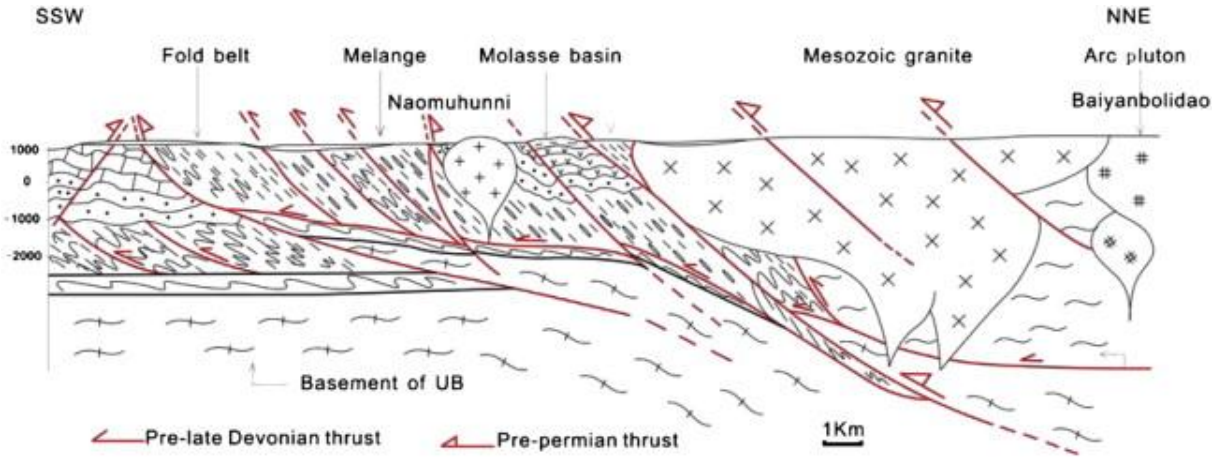


Fig. 7. Representative section of the NOB in Baiyanbaolidao area (according to mapping data of Xu et al., 1994; see Fig. 2 for location).

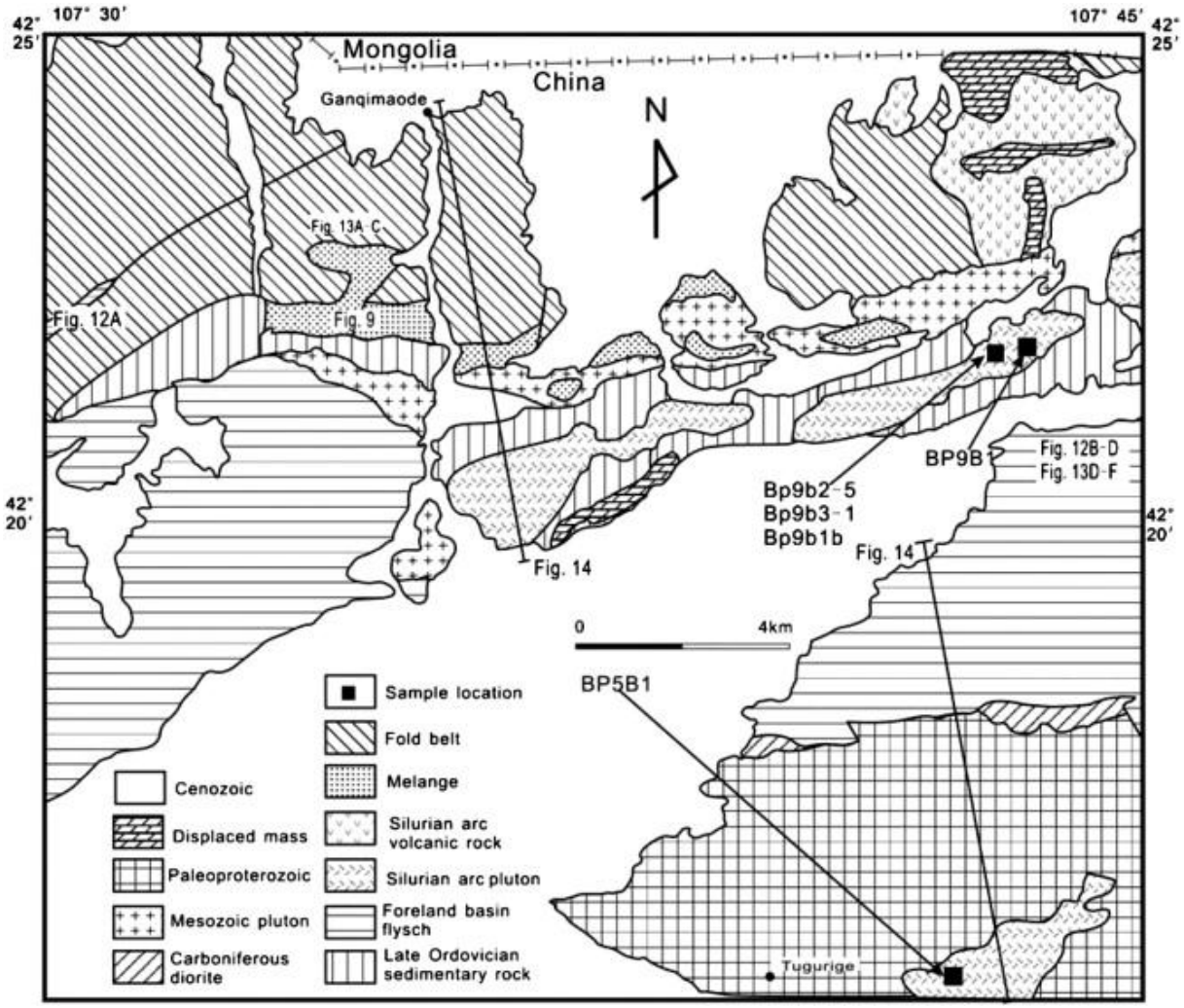


Fig. 8. Geological map showing the tectonic units of the SOB in Tugurige area (after Xu et al., 2001b). The section line of Fig. 14, locations of Fig. 9, Fig. 12 and Fig. 13 are marked (see Fig. 1C for location).

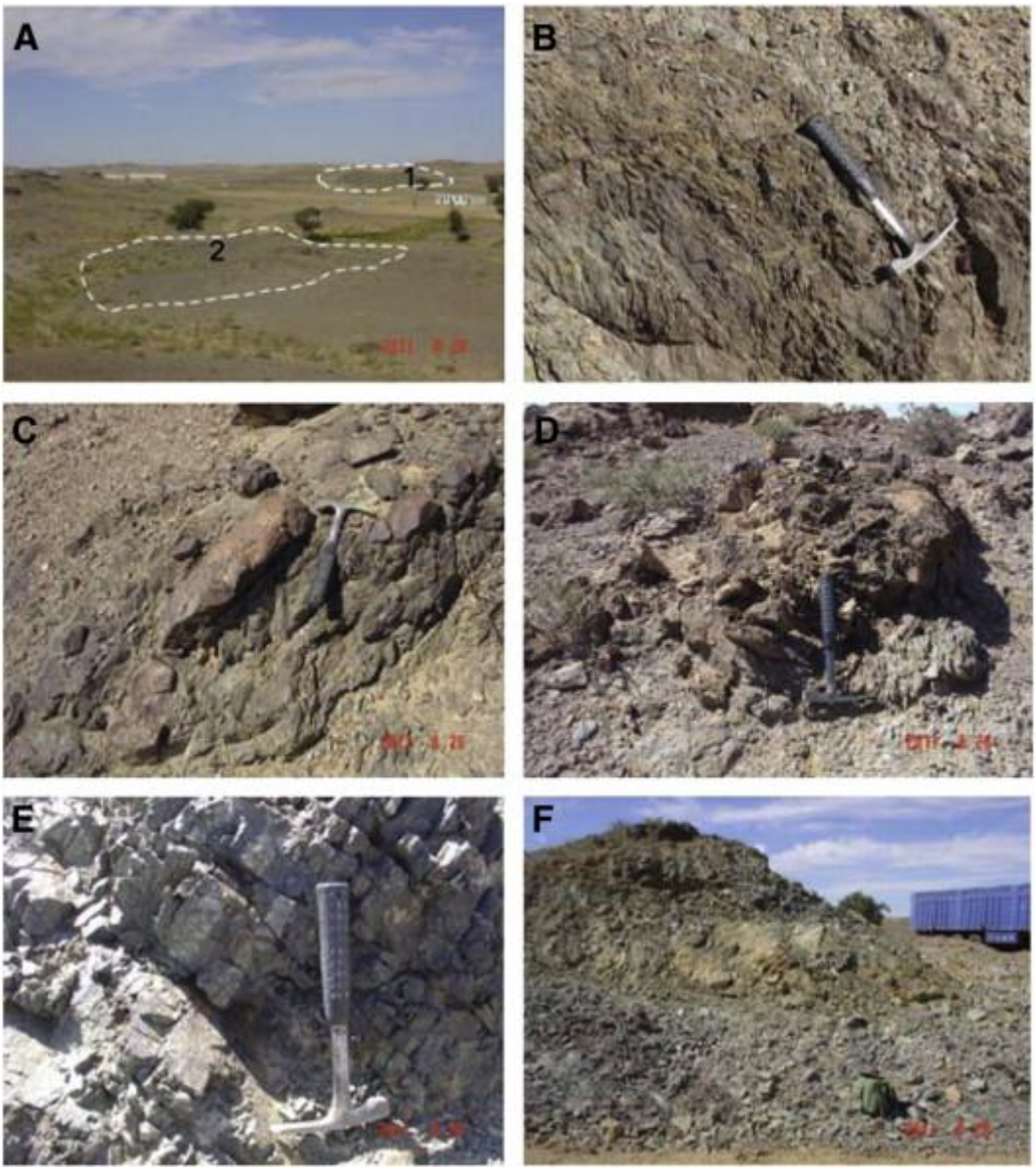


Fig. 9. Field features of the mélange belt in Ganqimaode. A: various kinds of blocks occur as small hills. Circle 1: mafic rock; Circle 2: hornblende schist; B: matrix showing a highly penetrative deformation and cataclastic texture; C: matrix-supported blocks texture, block is granite; D: ultramafic rock block; E: white mica schist block; F: hornblende schist block (see Fig. 8 for location).

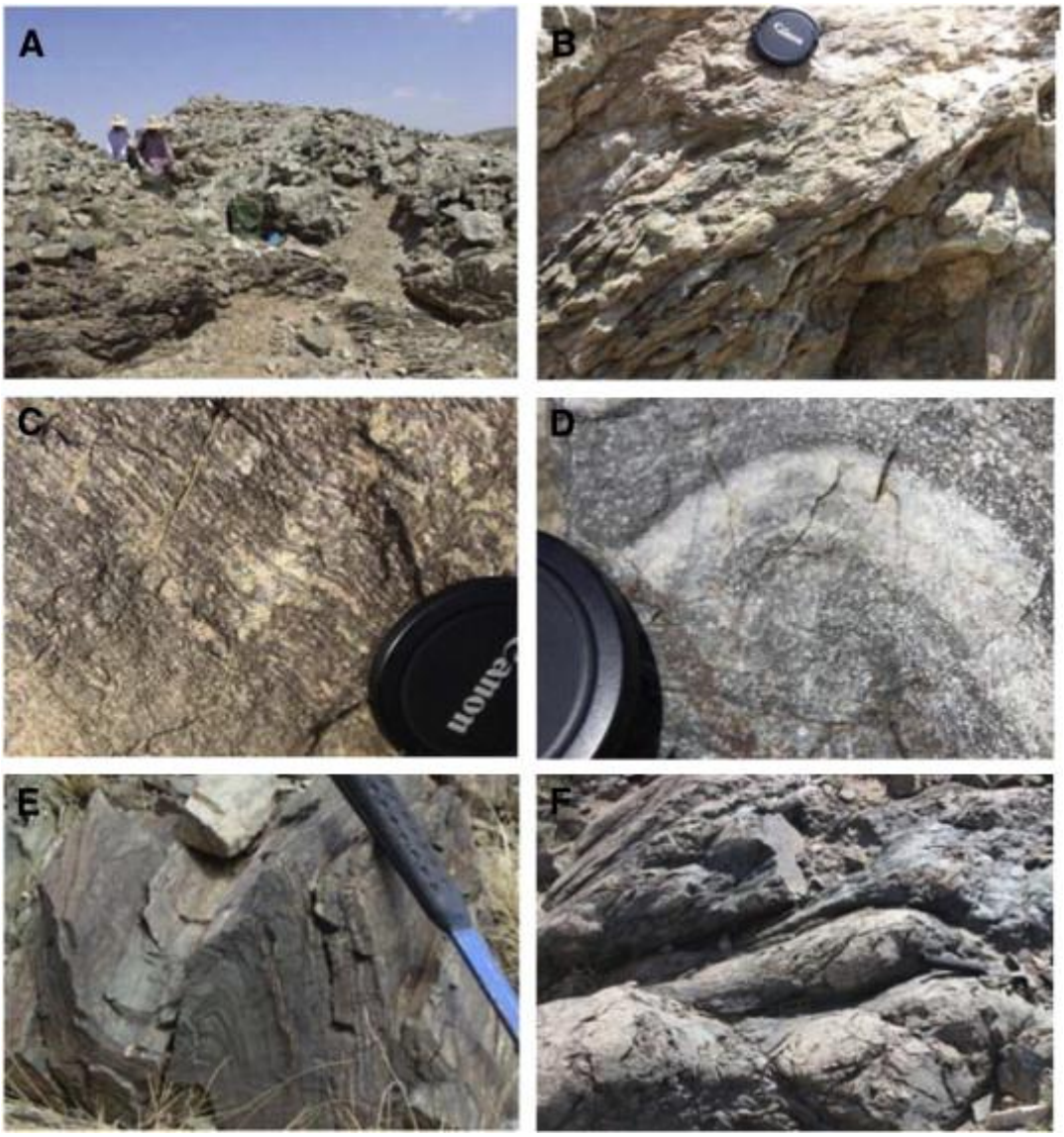


Fig. 10. Field features of the mélange belt in Bater area. A: ultramafic rock block; B: serpentinized ultramafic rock block, with a highly penetrative deformation; C: granitic mylonite; D: cataclastic texture in granitic mylonite; E: mylonitic schists, with small asymmetric folds; F: deformed pillow lava (see Fig. 1C for location).

Table 1. Chemical composition of diorites from Tugurige area.

| Sample | $SiO_2$ | $TiO_2$ | $Al_2O_3$ | $Fe_2O_3$ | FeO | MgO | MnO | CaO | $Na_2O$ | $K_2O$ | $P_2O_5$ | LOI | Total |
|---|---|---|---|---|---|---|---|---|---|---|---|---|---|
| Bp9b2-5 | 54.91 | 0.64 | 18.8 | 3.99 | 2.45 | 3.52 | 0.14 | 8.08 | 2.44 | 1.56 | 0.22 | 3.23 | 99.98 |
| Bp9b3-1 | 53.62 | 0.56 | 18.41 | 4.94 | 2.23 | 3.36 | 0.12 | 8.94 | 2.43 | 1.8 | 0.22 | 3.26 | 99.89 |
| Bp9b1b | 54.78 | 0.66 | 17.49 | 3.81 | 3.25 | 4.63 | 0.15 | 8.14 | 2.4 | 1.73 | 0.21 | 2.77 | 100.02 |

| | La | Ce | Pr | Nd | Sm | Eu | Gd | Tb | Dy | Ho | Er | Tm | Yb | Lu |
|---|---|---|---|---|---|---|---|---|---|---|---|---|---|---|
| Bp9b2-5 | 14.57 | 26.01 | 4.1 | 17.57 | 3.78 | 1.35 | 4.12 | 0.8 | 4.39 | 1.08 | 2.46 | 0.55 | 2.89 | 0.58 |
| Bp9b3-1 | 15.86 | 27.88 | 3.85 | 16.94 | 4.32 | 1.17 | 3.72 | 0.71 | 4.05 | 1.04 | 2.49 | 0.47 | 2.7 | 0.46 |
| Bp9b1b | 15.09 | 28.47 | 4.03 | 15.87 | 3.45 | 0.95 | 3.32 | 0.68 | 3.34 | 0.86 | 2.16 | 0.42 | 2.33 | 0.45 |

| | Y | Rb | Sr | Ba | Cs | Sc | Cr | Co | Ni | Cu | Zn | Sn | Zr | Hf | Nb | Ta | Pb | Th | U |
|---|---|---|---|---|---|---|---|---|---|---|---|---|---|---|---|---|---|---|---|
| Bp9b2-5 | 23.48 | 49.85 | 852.15 | 736.85 | 1.25 | 23.26 | 37.63 | 18.08 | 17.49 | 41.62 | 53.98 | 1.27 | 26.48 | 2.46 | 11.81 | 1.65 | 12.11 | 0.69 | 0.96 |
| Bp9b3-1 | 23.83 | 48.24 | 751.23 | 679.58 | 1.39 | 19.05 | 23.45 | 13.62 | 11.64 | 25.45 | 47.16 | 1.05 | 25.32 | 2.17 | 10.92 | 0.77 | 7.57 | 3.57 | 1.14 |
| Bp9b1b | 24.34 | 46.12 | 689 | 537.68 | 1.45 | 24.16 | 79.13 | 18.57 | 25.67 | 22.24 | 55.22 | 1.32 | 36.23 | 2.96 | 8.44 | | | | |

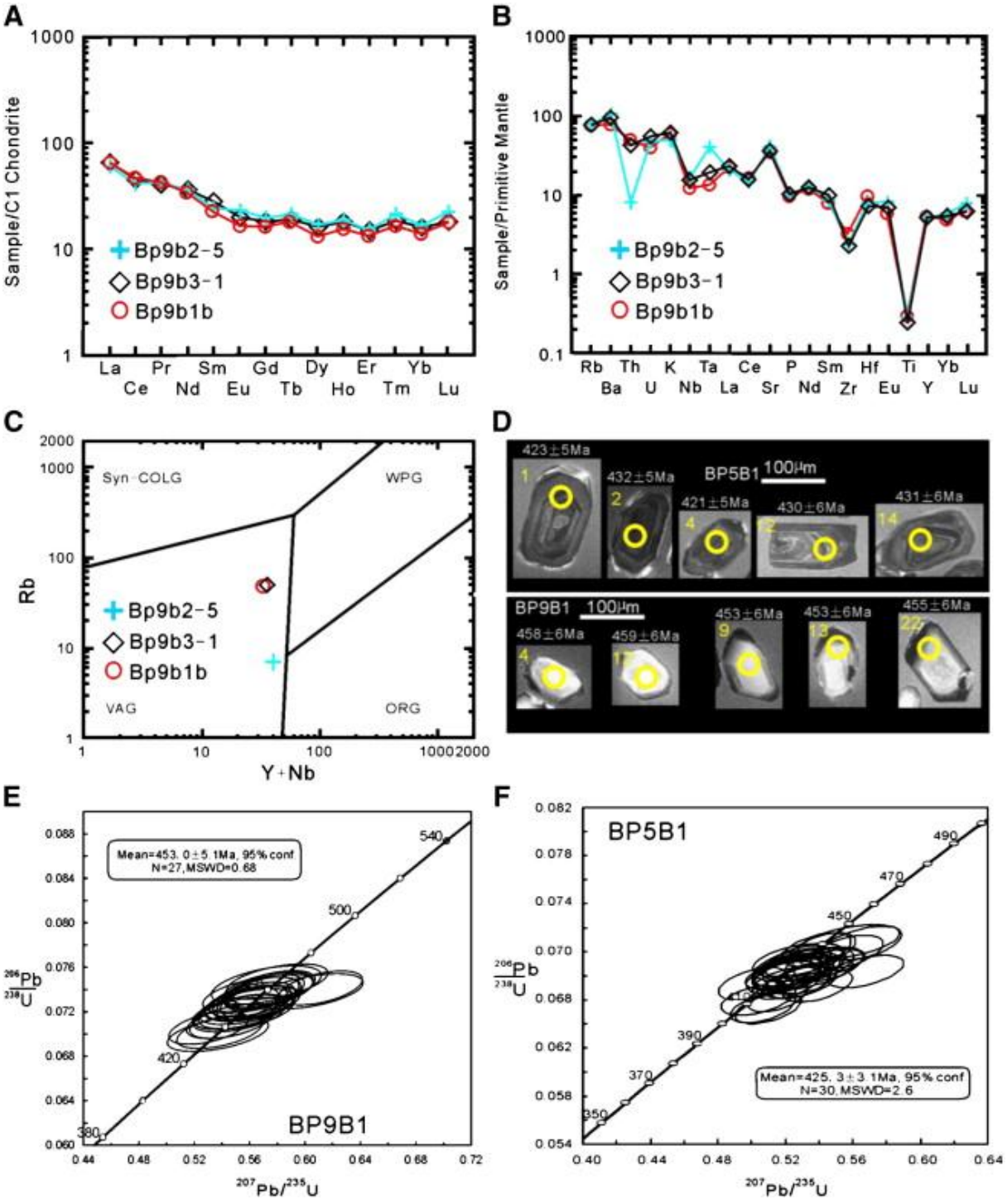


Fig. 11. Geochemical diagrams, Cathodoluminescence photographs and concordia diagrams of zircons of arc diorite belt in Tugurige area. A: chondrite-normalized REE diagram; B: primitive mantle-normalized spidergram. The normalization values are from Sun and McDonough (1989); C: geochemical-tectonic discrimination diagram (Pearce, 1984); D: Cathodoluminescence (CL) images; E and F: U–Pb zircon concordia diagrams for quartz diorites BP9B1 and BP5B1.

Table 2. LA-ICP-MS zircon U–Pb data for quartz diorites from Tugurige area.

| Spot number | Th (ppm) | U (ppm) | Th/U | Isotopic ratios | | | | | | Age (Ma) | |
|---|---|---|---|---|---|---|---|---|---|---|---|
| | | | | $^{207}Pb/^{206}Pb$ | 1σ | $^{207}Pb/^{235}U$ | 1σ | $^{206}Pb/^{238}U$ | 1σ | $^{206}Pb/^{238}U$ | 1σ |
| BP5B1-01 | 243.6 | 650.5 | 0.37 | 0.06 | 0 | 0.53 | 0.01 | 0.07 | 0 | 423 | 5 |
| BP5B1-02 | 280.2 | 632.3 | 0.44 | 0.06 | 0 | 0.53 | 0.02 | 0.07 | 0 | 432 | 5 |
| BP5B1-03 | 113.0 | 292.9 | 0.39 | 0.06 | 0 | 0.57 | 0.02 | 0.07 | 0 | 440 | 6 |
| BP5B1-04 | 369.7 | 678.1 | 0.55 | 0.06 | 0 | 0.53 | 0.01 | 0.07 | 0 | 421 | 5 |
| BP5B1-05 | 226.8 | 525.1 | 0.43 | 0.06 | 0 | 0.53 | 0.02 | 0.07 | 0 | 430 | 5 |
| BP5B1-06 | 207.5 | 493.8 | 0.42 | 0.06 | 0 | 0.54 | 0.01 | 0.07 | 0 | 437 | 5 |
| BP5B1-07 | 209.5 | 388.7 | 0.54 | 0.06 | 0 | 0.54 | 0.01 | 0.07 | 0 | 437 | 5 |
| BP5B1-08 | 167.2 | 349.1 | 0.48 | 0.06 | 0 | 0.56 | 0.02 | 0.07 | 0 | 441 | 6 |
| BP5B1-09 | 379.5 | 676.0 | 0.56 | 0.06 | 0 | 0.51 | 0.01 | 0.07 | 0 | 408 | 5 |
| BP5B1-10 | 491.1 | 847.4 | 0.58 | 0.06 | 0 | 0.52 | 0.01 | 0.07 | 0 | 414 | 5 |
| BP5B1-11 | 171.2 | 404.7 | 0.42 | 0.06 | 0 | 0.52 | 0.01 | 0.07 | 0 | 425 | 5 |
| BP5B1-12 | 93.7 | 256.0 | 0.37 | 0.06 | 0 | 0.54 | 0.02 | 0.07 | 0 | 430 | 6 |
| BP5B1-13 | 272.0 | 471.6 | 0.58 | 0.06 | 0 | 0.54 | 0.01 | 0.07 | 0 | 430 | 5 |
| BP5B1-14 | 187.7 | 433.4 | 0.43 | 0.06 | 0 | 0.53 | 0.01 | 0.07 | 0 | 431 | 5 |
| BP5B1-15 | 244.0 | 491.5 | 0.50 | 0.06 | 0 | 0.55 | 0.01 | 0.07 | 0 | 430 | 5 |
| BP5B1-16 | 120.9 | 294.0 | 0.41 | 0.06 | 0 | 0.52 | 0.02 | 0.07 | 0 | 427 | 5 |
| BP5B1-17 | 166.8 | 311.8 | 0.53 | 0.06 | 0 | 0.53 | 0.02 | 0.07 | 0 | 425 | 6 |
| BP5B1-18 | 195.4 | 511.7 | 0.38 | 0.06 | 0 | 0.53 | 0.01 | 0.07 | 0 | 421 | 5 |
| BP5B1-19 | 177.3 | 358.6 | 0.49 | 0.06 | 0 | 0.53 | 0.02 | 0.07 | 0 | 428 | 5 |
| BP5B1-20 | 379.5 | 593.0 | 0.64 | 0.06 | 0 | 0.56 | 0.01 | 0.07 | 0 | 436 | 5 |
| BP5B1-21 | 235.4 | 518.8 | 0.45 | 0.06 | 0 | 0.52 | 0.01 | 0.07 | 0 | 421 | 5 |
| BP5B1-22 | 217.1 | 512.1 | 0.42 | 0.06 | 0 | 0.57 | 0.01 | 0.07 | 0 | 426 | 5 |
| BP5B1-23 | 366.7 | 615.2 | 0.60 | 0.06 | 0 | 0.54 | 0.01 | 0.07 | 0 | 419 | 5 |
| BP5B1-24 | 386.4 | 765.9 | 0.50 | 0.06 | 0 | 0.51 | 0.01 | 0.07 | 0 | 408 | 5 |
| BP5B1-25 | 319.3 | 484.8 | 0.66 | 0.06 | 0 | 0.53 | 0.02 | 0.07 | 0 | 427 | 5 |
| BP5B1-26 | 116.0 | 452.4 | 0.26 | 0.06 | 0 | 0.5 | 0.01 | 0.07 | 0 | 412 | 5 |
| BP5B1-27 | 126.3 | 395.8 | 0.32 | 0.06 | 0 | 0.52 | 0.01 | 0.07 | 0 | 425 | 5 |
| BP5B1-28 | 228.9 | 395.2 | 0.58 | 0.05 | 0 | 0.5 | 0.01 | 0.07 | 0 | 420 | 5 |
| BP5B1-29 | 91.1 | 404.1 | 0.23 | 0.06 | 0 | 0.52 | 0.01 | 0.07 | 0 | 423 | 5 |
| BP5B1-30 | 222.2 | 422.8 | 0.53 | 0.06 | 0 | 0.52 | 0.01 | 0.07 | 0 | 424 | 5 |
| BP9B1-01 | 40.0 | 106.4 | 0.38 | 0.06 | 0 | 0.58 | 0.02 | 0.07 | 0 | 464 | 6 |
| BP9B1-02 | 38.3 | 93.7 | 0.41 | 0.06 | 0 | 0.56 | 0.02 | 0.07 | 0 | 453 | 6 |
| BP9B1-03 | 153.8 | 154.7 | 0.99 | 0.06 | 0 | 0.84 | 0.03 | 0.1 | 0 | 617 | 8 |
| BP9B1-04 | 95.2 | 170.5 | 0.56 | 0.06 | 0 | 0.57 | 0.02 | 0.07 | 0 | 458 | 6 |
| BP9B1-05 | 174.6 | 305.2 | 0.57 | 0.06 | 0 | 0.56 | 0.02 | 0.07 | 0 | 454 | 6 |
| BP9B1-06 | 54.5 | 119.0 | 0.46 | 0.06 | 0 | 0.58 | 0.02 | 0.07 | 0 | 461 | 6 |
| BP9B1-07 | 46.9 | 139.1 | 0.34 | 0.06 | 0 | 0.57 | 0.02 | 0.07 | 0 | 459 | 6 |
| BP9B1-08 | 73.7 | 137.6 | 0.54 | 0.06 | 0 | 0.55 | 0.02 | 0.07 | 0 | 453 | 6 |
| BP9B1-09 | 65.0 | 145.0 | 0.45 | 0.06 | 0 | 0.56 | 0.02 | 0.07 | 0 | 453 | 6 |
| BP9B1-10 | 70.7 | 120.1 | 0.59 | 0.07 | 0 | 0.66 | 0.04 | 0.07 | 0 | 455 | 7 |
| BP9B1-11 | 49.6 | 128.1 | 0.39 | 0.06 | 0 | 0.69 | 0.04 | 0.08 | 0 | 495 | 7 |
| BP9B1-12 | 84.7 | 169.3 | 0.50 | 0.06 | 0 | 0.57 | 0.02 | 0.07 | 0 | 459 | 6 |
| BP9B1-13 | 47.5 | 139.2 | 0.34 | 0.06 | 0 | 0.56 | 0.02 | 0.07 | 0 | 453 | 6 |
| BP9B1-14 | 92.2 | 223.7 | 0.41 | 0.06 | 0 | 0.61 | 0.02 | 0.07 | 0 | 461 | 6 |
| BP9B1-15 | 32.6 | 99.6 | 0.33 | 0.06 | 0 | 0.6 | 0.03 | 0.07 | 0 | 459 | 6 |
| BP9B1-16 | 46.6 | 102.2 | 0.46 | 0.06 | 0 | 0.57 | 0.02 | 0.07 | 0 | 460 | 6 |
| BP9B1-17 | 40.6 | 112.3 | 0.36 | 0.06 | 0 | 0.54 | 0.02 | 0.07 | 0 | 437 | 6 |

| Spot number | Th (ppm) | U (ppm) | Th/U | Isotopic ratios | | | | | | Age (Ma) | |
|---|---|---|---|---|---|---|---|---|---|---|---|
| | | | | $^{207}Pb/^{206}Pb$ | 1σ | $^{207}Pb/^{235}U$ | 1σ | $^{206}Pb/^{238}U$ | 1σ | $^{206}Pb/^{238}U$ | 1σ |
| BP9B1-18 | 47.2 | 114.1 | 0.41 | 0.06 | 0 | 0.55 | 0.02 | 0.07 | 0 | 448 | 6 |
| BP9B1-19 | 41.4 | 111.8 | 0.37 | 0.06 | 0 | 0.56 | 0.02 | 0.07 | 0 | 452 | 6 |
| BP9B1-20 | 43.4 | 106.1 | 0.41 | 0.06 | 0 | 0.56 | 0.02 | 0.07 | 0 | 448 | 6 |
| BP9B1-21 | 38.6 | 107.0 | 0.36 | 0.06 | 0 | 0.55 | 0.02 | 0.07 | 0 | 443 | 6 |
| BP9B1-22 | 46.2 | 131.8 | 0.35 | 0.06 | 0 | 0.56 | 0.02 | 0.07 | 0 | 455 | 6 |
| BP9B1-23 | 49.2 | 108.6 | 0.45 | 0.06 | 0 | 0.55 | 0.02 | 0.07 | 0 | 447 | 6 |
| BP9B1-24 | 61.9 | 136.8 | 0.45 | 0.06 | 0 | 0.55 | 0.02 | 0.07 | 0 | 448 | 6 |
| BP9B1-25 | 57.8 | 123.0 | 0.47 | 0.06 | 0 | 0.55 | 0.02 | 0.07 | 0 | 443 | 6 |
| BP9B1-26 | 40.1 | 92.5 | 0.43 | 0.06 | 0 | 0.57 | 0.03 | 0.07 | 0 | 463 | 7 |
| BP9B1-27 | 48.8 | 98.8 | 0.49 | 0.06 | 0 | 0.56 | 0.02 | 0.07 | 0 | 451 | 6 |
| BP9B1-28 | 45.1 | 108.8 | 0.41 | 0.06 | 0 | 0.56 | 0.02 | 0.07 | 0 | 457 | 6 |
| BP9B1-29 | 97.8 | 180.1 | 0.54 | 0.05 | 0 | 0.53 | 0.02 | 0.07 | 0 | 440 | 6 |
| BP9B1-30 | 58.5 | 125.6 | 0.47 | 0.06 | 0 | 0.54 | 0.02 | 0.07 | 0 | 436 | 6 |


Fig. 12. Field features of flysch and molasse in foreland basin of the SOB. A: unconformity between the Xuniwusu Formation and the underlying Ondor Sum Group; B: upward fining coarse cycles in lower part of the Xuniwusu Formation flysch; C: $T_{ae}$ Bouma sequences; D: upward fining cycles of typical Bouma sequence in upper part of the Xuniwusu Formation flysch; E: three conglomerate-sandstone cycles (red lines in photograph) in lower part of the Xibiehe Formation; F: red conglomerate of the Xibiehe Formation, Bater area; G: thick conglomerate and H: middle-sized inclined bedding of the Xibiehe Formation, Ondor Sum area. (see Fig. 8 for location). (For interpretation of the references to color in this figure legend, the reader is referred to the web version of this article.)

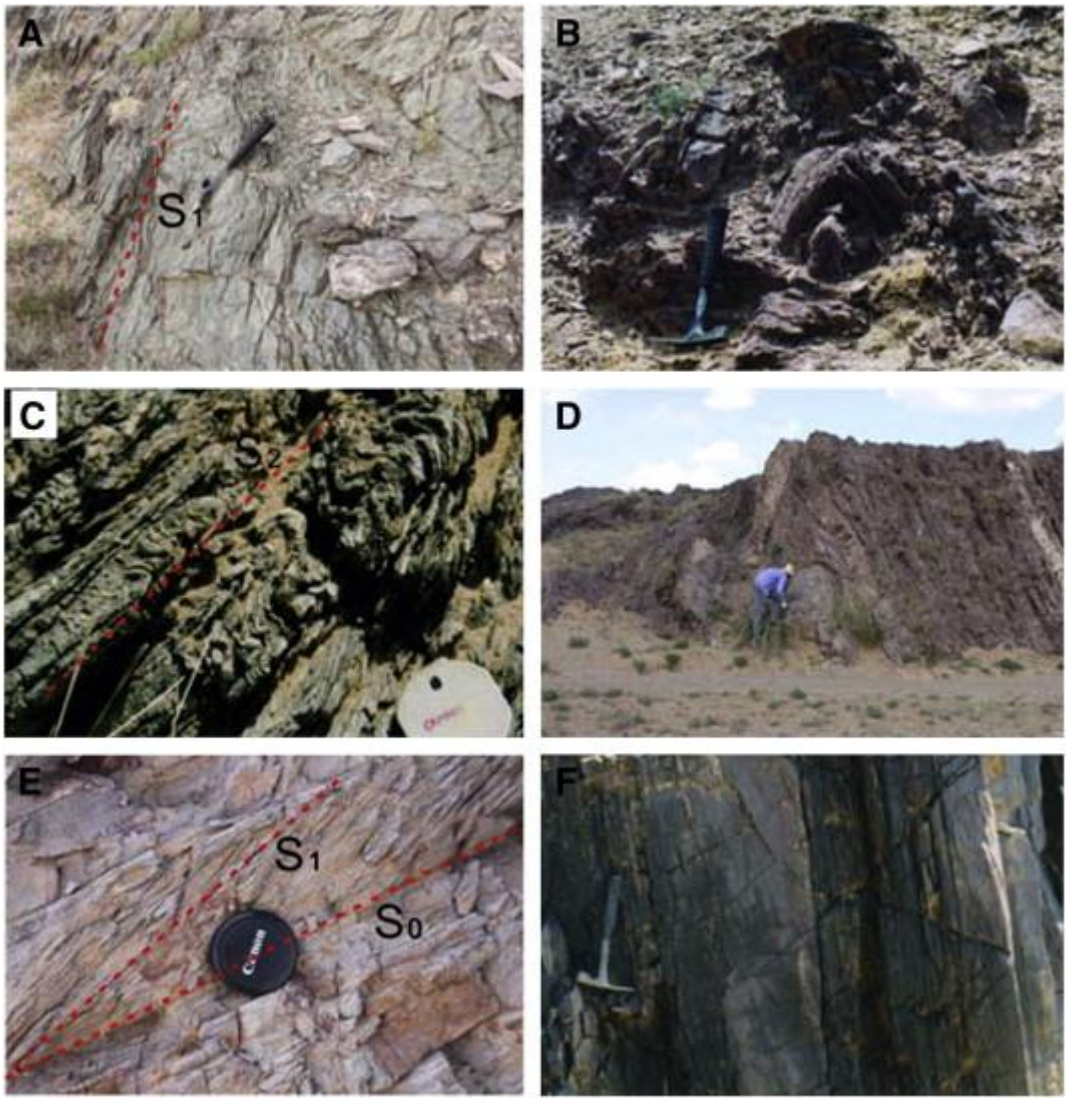


Fig. 13. Representative deformation features in fold belt and foreland basin of the SOB in Tugurige area. A: penetrative foliations ($S_1$) of the Ondor Sum Group; B: outcrop-scale folds of the Ondor Sum Group; C: zonal crenulation cleavage ($S_2$) forming 2–10 cm thick microlithons of the Ondor Sum Group; D: northward overturned folds with middle to high angle south-dipping axial-plane cleavage (S1), Xuniwusu Formation; E: axial-plane cleavage ($S_1$) that cut bedding ($S_0$), Xuniwusu Formation; F: axial-plane cleavage ($S_1$) not displacing bedding and preserving the graded bedding of the Bouma sequence (see Fig. 8 for location).

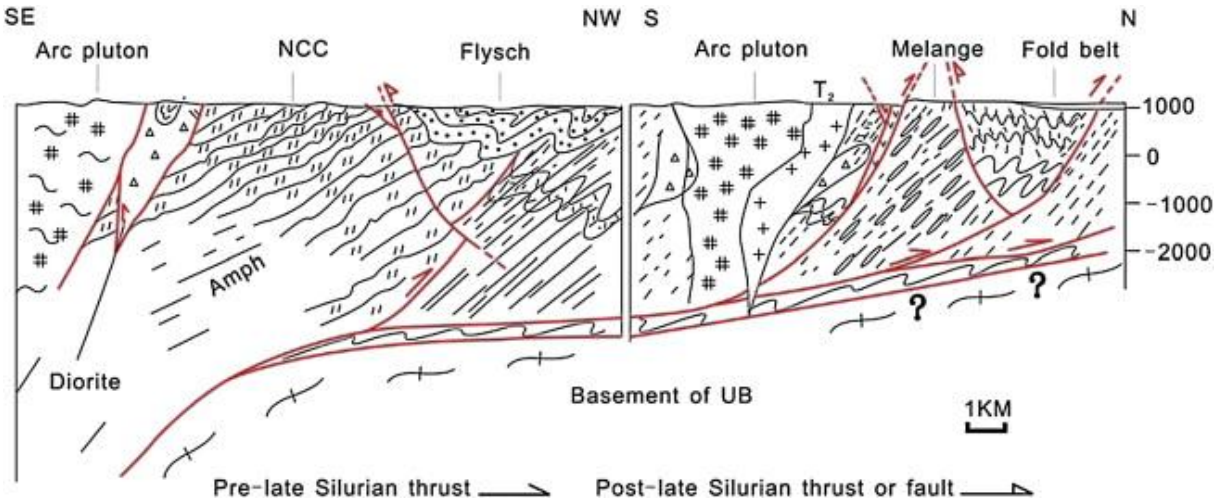


Fig. 14. Representative section of the SOB in Tugurige area (according to Xu et al., 2001b, see Fig. 8 for location; same remark as for Fig. 7).

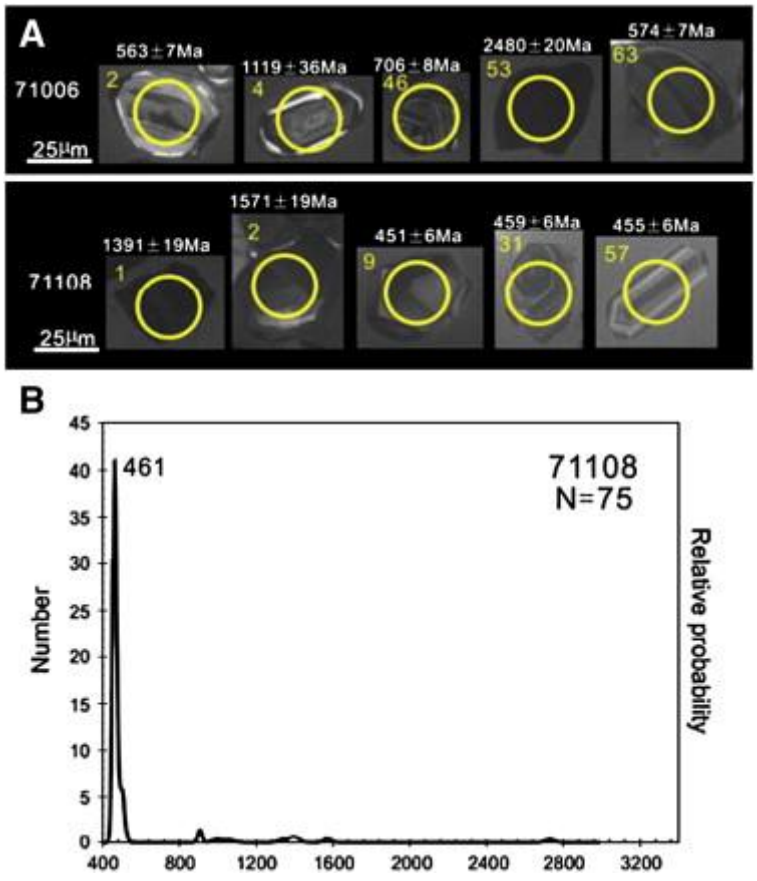


Fig. 15. Cathodoluminescence photographs and probability plots of zircons of sample. A: cathodoluminescence photographs of 71006 and 71108; B: probability plots of 71108.

Table 3. LA-ICP-MS zircon U–Pb data for sandstones from Tugurige and Baiyanbolidao areas.

| Spot number | Th (ppm) | U (ppm) | Th/U | Isotopic ratios | | | | | | Age (Ma) | | | |
|---|---|---|---|---|---|---|---|---|---|---|---|---|---|
| | | | | $^{207}Pb/^{206}Pb$ | 1σ | $^{207}Pb/^{235}U$ | 1σ | $^{206}Pb/^{238}U$ | 1σ | $^{207}Pb/^{206}Pb$ | 1σ | $^{206}Pb/^{238}U$ | 1σ |
| 71108-01 | 203.9 | 507.6 | 0.40 | 0.09 | 0 | 3.09 | 0.06 | 0.25 | 0 | 1391 | 19 | 1456 | 16 |
| 71108-02 | 162.5 | 227.5 | 0.71 | 0.1 | 0 | 3.76 | 0.07 | 0.28 | 0 | 1571 | 19 | 1594 | 18 |
| 71108-03 | 413.5 | 354.0 | 1.17 | 0.06 | 0 | 0.65 | 0.01 | 0.08 | 0 | 479 | 26 | 513 | 6 |
| 71108-04 | 115.7 | 158.6 | 0.73 | 0.06 | 0 | 0.59 | 0.01 | 0.08 | 0 | 454 | 26 | 473 | 6 |
| 71108-05 | 52.6 | 146.4 | 0.36 | 0.06 | 0 | 0.67 | 0.02 | 0.08 | 0 | 495 | 30 | 525 | 7 |
| 71108-06 | 143.2 | 259.9 | 0.55 | 0.06 | 0 | 0.57 | 0.02 | 0.07 | 0 | 463 | 36 | 457 | 6 |
| 71108-07 | 60.3 | 77.1 | 0.78 | 0.06 | 0 | 0.55 | 0.02 | 0.07 | 0 | 445 | 63 | 442 | 6 |
| 71108-08 | 104.4 | 170.8 | 0.61 | 0.06 | 0 | 0.56 | 0.02 | 0.07 | 0 | 456 | 43 | 455 | 6 |
| 71108-09 | 127.6 | 197.4 | 0.65 | 0.05 | 0 | 0.55 | 0.01 | 0.07 | 0 | 408 | 36 | 451 | 6 |
| 71108-10 | 27.5 | 74.1 | 0.37 | 0.06 | 0 | 0.59 | 0.02 | 0.08 | 0 | 465 | 65 | 469 | 6 |
| 71108-11 | 143.8 | 338.1 | 0.43 | 0.06 | 0 | 0.58 | 0.01 | 0.08 | 0 | 458 | 28 | 467 | 6 |
| 71108-12 | 112.2 | 178.8 | 0.63 | 0.06 | 0 | 0.61 | 0.02 | 0.08 | 0 | 466 | 37 | 489 | 6 |
| 71108-13 | 210.8 | 320.5 | 0.66 | 0.06 | 0 | 0.57 | 0.01 | 0.07 | 0 | 442 | 29 | 460 | 6 |
| 71108-14 | 218.4 | 442.9 | 0.49 | 0.06 | 0 | 0.54 | 0.01 | 0.07 | 0 | 413 | 29 | 447 | 6 |
| 71108-15 | 65.7 | 111.5 | 0.59 | 0.06 | 0 | 0.58 | 0.02 | 0.07 | 0 | 469 | 52 | 461 | 6 |
| 71108-16 | 173.2 | 329.6 | 0.53 | 0.06 | 0 | 0.63 | 0.01 | 0.08 | 0 | 494 | 28 | 498 | 6 |
| 71108-17 | 118.8 | 124.7 | 0.95 | 0.06 | 0 | 0.57 | 0.02 | 0.07 | 0 | 454 | 36 | 459 | 6 |
| 71108-18 | 67.7 | 120.3 | 0.56 | 0.06 | 0 | 0.58 | 0.02 | 0.08 | 0 | 461 | 42 | 468 | 6 |
| 71108-19 | 60.3 | 101.6 | 0.59 | 0.06 | 0 | 0.59 | 0.02 | 0.08 | 0 | 477 | 39 | 473 | 6 |
| 71108-20 | 196.0 | 222.6 | 0.88 | 0.06 | 0 | 0.56 | 0.01 | 0.07 | 0 | 443 | 31 | 456 | 6 |
| 71108-21 | 151.6 | 235.0 | 0.65 | 0.06 | 0 | 0.57 | 0.02 | 0.07 | 0 | 454 | 36 | 457 | 6 |
| 71108-22 | 84.1 | 166.2 | 0.51 | 0.06 | 0 | 0.58 | 0.02 | 0.08 | 0 | 448 | 35 | 469 | 6 |
| 71108-23 | 169.2 | 316.2 | 0.54 | 0.06 | 0 | 0.57 | 0.01 | 0.07 | 0 | 416 | 30 | 464 | 6 |
| 71108-24 | 111.7 | 211.1 | 0.53 | 0.06 | 0 | 0.6 | 0.02 | 0.08 | 0 | 478 | 35 | 479 | 6 |
| 71108-25 | 128.2 | 480.9 | 0.27 | 0.07 | 0 | 1.75 | 0.04 | 0.18 | 0 | 994 | 24 | 1043 | 12 |
| 71108-26 | 491.6 | 655.0 | 0.75 | 0.06 | 0 | 0.58 | 0.01 | 0.08 | 0 | 424 | 28 | 473 | 6 |
| 71108-27 | 169.8 | 293.1 | 0.58 | 0.06 | 0 | 0.59 | 0.01 | 0.08 | 0 | 445 | 31 | 478 | 6 |
| 71108-28 | 67.8 | 102.2 | 0.66 | 0.06 | 0 | 0.59 | 0.02 | 0.08 | 0 | 461 | 46 | 473 | 6 |
| 71108-29 | 112.1 | 167.5 | 0.67 | 0.06 | 0 | 0.6 | 0.02 | 0.08 | 0 | 473 | 36 | 477 | 6 |
| 71108-30 | 435.0 | 520.1 | 0.84 | 0.06 | 0 | 0.56 | 0.01 | 0.07 | 0 | 420 | 29 | 456 | 6 |
| 71108-31 | 85.2 | 122.1 | 0.70 | 0.06 | 0 | 0.57 | 0.02 | 0.07 | 0 | 457 | 39 | 459 | 6 |
| 71108-32 | 166.4 | 177.2 | 0.94 | 0.09 | 0 | 3.02 | 0.07 | 0.25 | 0 | 1409 | 23 | 1416 | 16 |
| 71108-33 | 178.1 | 195.3 | 0.91 | 0.06 | 0 | 0.56 | 0.01 | 0.07 | 0 | 441 | 35 | 456 | 6 |
| 71108-34 | 94.6 | 154.9 | 0.61 | 0.06 | 0 | 0.56 | 0.02 | 0.07 | 0 | 442 | 39 | 456 | 6 |
| 71108-35 | 241.4 | 295.3 | 0.82 | 0.06 | 0 | 0.55 | 0.01 | 0.07 | 0 | 416 | 32 | 451 | 6 |
| 71108-36 | 92.0 | 148.3 | 0.62 | 0.06 | 0 | 0.56 | 0.02 | 0.07 | 0 | 456 | 37 | 451 | 6 |
| 71108-37 | 129.0 | 227.3 | 0.57 | 0.09 | 0 | 2.6 | 0.06 | 0.22 | 0 | 1338 | 24 | 1277 | 15 |
| 71108-38 | 50.7 | 132.0 | 0.38 | 0.06 | 0 | 0.64 | 0.02 | 0.08 | 0 | 498 | 41 | 500 | 6 |
| 71108-39 | 88.1 | 164.8 | 0.53 | 0.06 | 0 | 0.57 | 0.02 | 0.07 | 0 | 455 | 36 | 458 | 6 |
| 71108-40 | 33.8 | 116.9 | 0.29 | 0.07 | 0 | 1.48 | 0.04 | 0.15 | 0 | 963 | 30 | 906 | 11 |
| 71108-41 | 107.8 | 163.3 | 0.66 | 0.06 | 0 | 0.58 | 0.02 | 0.08 | 0 | 465 | 36 | 467 | 6 |
| 71108-42 | 204.3 | 228.3 | 0.89 | 0.06 | 0 | 0.57 | 0.01 | 0.07 | 0 | 460 | 34 | 456 | 6 |
| 71108-43 | 222.4 | 422.7 | 0.53 | 0.06 | 0 | 0.61 | 0.01 | 0.08 | 0 | 483 | 31 | 484 | 6 |
| 71108-44 | 137.5 | 209.5 | 0.66 | 0.06 | 0 | 0.57 | 0.02 | 0.07 | 0 | 448 | 35 | 464 | 6 |
| 71108-45 | 76.4 | 162.9 | 0.47 | 0.06 | 0 | 0.58 | 0.02 | 0.08 | 0 | 450 | 38 | 468 | 6 |
| 71108-46 | 45.6 | 86.5 | 0.53 | 0.06 | 0 | 0.58 | 0.02 | 0.08 | 0 | 461 | 58 | 469 | 6 |

| Spot number | Th (ppm) | U (ppm) | Th/U | Isotopic ratios | | | | | | Age (Ma) | | | |
|---|---|---|---|---|---|---|---|---|---|---|---|---|---|
| | | | | $^{207}Pb/^{206}Pb$ | 1σ | $^{207}Pb/^{235}U$ | 1σ | $^{206}Pb/^{238}U$ | 1σ | $^{207}Pb/^{206}Pb$ | 1σ | $^{206}Pb/^{238}U$ | 1σ |
| 71108-47 | 190.3 | 197.5 | 0.96 | 0.06 | 0 | 0.58 | 0.02 | 0.08 | 0 | 424 | 36 | 473 | 6 |
| 71108-48 | 181.2 | 280.2 | 0.65 | 0.06 | 0 | 0.56 | 0.01 | 0.07 | 0 | 414 | 33 | 463 | 6 |
| 71108-49 | 264.7 | 341.7 | 0.77 | 0.06 | 0 | 0.58 | 0.01 | 0.08 | 0 | 442 | 34 | 471 | 6 |
| 71108-50 | 447.1 | 273.6 | 1.63 | 0.07 | 0 | 1.94 | 0.05 | 0.19 | 0 | 1059 | 27 | 1112 | 13 |
| 71108-51 | 66.9 | 162.1 | 0.41 | 0.06 | 0 | 0.64 | 0.02 | 0.08 | 0 | 501 | 41 | 506 | 6 |
| 71108-52 | 64.6 | 129.1 | 0.50 | 0.07 | 0 | 1.43 | 0.04 | 0.15 | 0 | 879 | 32 | 908 | 11 |
| 71108-53 | 152.7 | 256.1 | 0.60 | 0.06 | 0 | 0.57 | 0.01 | 0.07 | 0 | 459 | 35 | 459 | 6 |
| 71108-54 | 156.4 | 213.3 | 0.73 | 0.06 | 0 | 0.58 | 0.02 | 0.07 | 0 | 467 | 38 | 465 | 6 |
| 71108-55 | 95.0 | 158.3 | 0.60 | 0.06 | 0 | 0.56 | 0.02 | 0.07 | 0 | 428 | 40 | 460 | 6 |
| 71108-56 | 144.8 | 207.2 | 0.70 | 0.06 | 0 | 0.56 | 0.01 | 0.07 | 0 | 445 | 35 | 453 | 6 |
| 71108-57 | 81.9 | 120.4 | 0.68 | 0.06 | 0 | 0.58 | 0.02 | 0.07 | 0 | 463 | 45 | 465 | 6 |
| 71108-58 | 88.8 | 177.2 | 0.50 | 0.06 | 0 | 0.58 | 0.02 | 0.08 | 0 | 444 | 37 | 470 | 6 |
| 71108-59 | 83.6 | 135.9 | 0.61 | 0.06 | 0 | 0.61 | 0.02 | 0.08 | 0 | 494 | 44 | 485 | 6 |
| 71108-60 | 82.1 | 137.6 | 0.60 | 0.06 | 0 | 0.58 | 0.02 | 0.07 | 0 | 450 | 43 | 465 | 6 |
| 71108-61 | 223.6 | 273.9 | 0.82 | 0.05 | 0 | 0.54 | 0.01 | 0.07 | 0 | 402 | 35 | 445 | 6 |
| 71108-62 | 119.7 | 210.2 | 0.57 | 0.06 | 0 | 0.56 | 0.02 | 0.07 | 0 | 452 | 42 | 453 | 6 |
| 71108-63 | 108.5 | 179.4 | 0.61 | 0.06 | 0 | 0.57 | 0.02 | 0.07 | 0 | 423 | 41 | 465 | 6 |
| 71108-64 | 117.3 | 143.8 | 0.82 | 0.06 | 0 | 0.57 | 0.02 | 0.07 | 0 | 459 | 41 | 456 | 6 |
| 71108-65 | 136.8 | 291.3 | 0.47 | 0.06 | 0 | 0.57 | 0.02 | 0.07 | 0 | 448 | 37 | 459 | 6 |
| 71108-66 | 109.2 | 149.0 | 0.73 | 0.06 | 0 | 0.62 | 0.02 | 0.08 | 0 | 507 | 40 | 490 | 6 |
| 71108-67 | 91.5 | 126.8 | 0.72 | 0.19 | 0 | 12.88 | 0.32 | 0.5 | 0.01 | 2729 | 24 | 2595 | 28 |
| 71108-68 | 176.8 | 219.9 | 0.80 | 0.06 | 0 | 0.56 | 0.02 | 0.07 | 0 | 435 | 41 | 457 | 6 |
| 71108-69 | 137.9 | 178.5 | 0.77 | 0.06 | 0 | 0.57 | 0.02 | 0.07 | 0 | 458 | 39 | 462 | 6 |
| 71108-70 | 123.6 | 295.5 | 0.42 | 0.06 | 0 | 0.57 | 0.02 | 0.07 | 0 | 471 | 37 | 458 | 6 |
| 71108-71 | 134.8 | 188.1 | 0.72 | 0.06 | 0 | 0.58 | 0.02 | 0.07 | 0 | 463 | 40 | 465 | 6 |
| 71108-72 | 121.5 | 132.9 | 0.91 | 0.06 | 0 | 0.58 | 0.02 | 0.08 | 0 | 456 | 50 | 468 | 6 |
| 71108-73 | 98.3 | 223.6 | 0.44 | 0.06 | 0 | 0.63 | 0.02 | 0.08 | 0 | 489 | 38 | 500 | 6 |
| 71108-74 | 170.0 | 164.4 | 1.03 | 0.06 | 0 | 0.63 | 0.02 | 0.08 | 0 | 440 | 40 | 509 | 6 |
| 71108-75 | 99.7 | 136.8 | 0.73 | 0.05 | 0 | 0.57 | 0.02 | 0.08 | 0 | 392 | 45 | 472 | 6 |
| 71006-01 | 167.8 | 268.0 | 0.63 | 0.07 | 0 | 1.77 | 0.04 | 0.17 | 0 | 1040 | 30 | 1032 | 12 |
| 71006-02 | 96.4 | 168.3 | 0.57 | 0.06 | 0 | 0.74 | 0.02 | 0.09 | 0 | 566 | 42 | 563 | 7 |
| 71006-03 | 1370.5 | 707.8 | 1.94 | 0.09 | 0 | 2.1 | 0.04 | 0.17 | 0 | 1386 | 21 | 1028 | 11 |
| 71006-04 | 245.1 | 153.6 | 1.60 | 0.08 | 0 | 2 | 0.06 | 0.19 | 0 | 1119 | 36 | 1115 | 13 |
| 71006-05 | 134.2 | 219.5 | 0.61 | 0.07 | 0 | 1.63 | 0.04 | 0.16 | 0 | 979 | 26 | 983 | 11 |
| 71006-06 | 529.7 | 862.2 | 0.61 | 0.14 | 0 | 5.32 | 0.1 | 0.27 | 0 | 2279 | 17 | 1527 | 16 |
| 71006-07 | 119.1 | 204.8 | 0.58 | 0.06 | 0 | 0.8 | 0.02 | 0.1 | 0 | 592 | 37 | 595 | 7 |
| 71006-08 | 529.0 | 769.3 | 0.69 | 0.07 | 0 | 1.5 | 0.03 | 0.15 | 0 | 989 | 23 | 903 | 10 |
| 71006-09 | 147.5 | 566.3 | 0.26 | 0.21 | 0 | 13.44 | 0.25 | 0.46 | 0.01 | 2935 | 16 | 2420 | 24 |
| 71006-10 | 441.4 | 312.0 | 1.41 | 0.06 | 0 | 0.76 | 0.02 | 0.09 | 0 | 574 | 32 | 574 | 7 |
| 71006-11 | 314.2 | 143.6 | 2.19 | 0.11 | 0 | 4.54 | 0.1 | 0.31 | 0 | 1746 | 22 | 1730 | 18 |
| 71006-12 | 113.4 | 156.0 | 0.73 | 0.09 | 0 | 2.08 | 0.06 | 0.17 | 0 | 1427 | 31 | 1000 | 12 |
| 71006-13 | 498.0 | 205.1 | 2.43 | 0.06 | 0 | 0.8 | 0.02 | 0.1 | 0 | 597 | 37 | 599 | 7 |
| 71006-14 | 271.3 | 235.3 | 1.15 | 0.07 | 0 | 1.83 | 0.04 | 0.18 | 0 | 1063 | 28 | 1050 | 12 |
| 71006-15 | 86.0 | 170.6 | 0.50 | 0.07 | 0 | 1.61 | 0.04 | 0.16 | 0 | 979 | 33 | 970 | 11 |
| 71006-16 | 134.0 | 206.0 | 0.65 | 0.11 | 0 | 3.75 | 0.08 | 0.25 | 0 | 1802 | 21 | 1421 | 15 |
| 71006-17 | 84.9 | 136.6 | 0.62 | 0.07 | 0 | 1.61 | 0.05 | 0.16 | 0 | 968 | 41 | 975 | 11 |
| 71006-18 | 130.8 | 208.7 | 0.63 | 0.08 | 0 | 2.67 | 0.06 | 0.23 | 0 | 1302 | 22 | 1331 | 14 |
| 71006-19 | 763.0 | 374.7 | 2.04 | 0.16 | 0 | 7.8 | 0.16 | 0.36 | 0 | 2445 | 18 | 1963 | 20 |
| 71006-20 | 207.4 | 522.9 | 0.40 | 0.07 | 0 | 1.76 | 0.04 | 0.17 | 0 | 1038 | 23 | 1028 | 11 |

| Spot number | Th (ppm) | U (ppm) | Th/U | Isotopic ratios | | | | | | Age (Ma) | | | |
|---|---|---|---|---|---|---|---|---|---|---|---|---|---|
| | | | | $^{207}Pb/^{206}Pb$ | 1σ | $^{207}Pb/^{235}U$ | 1σ | $^{206}Pb/^{238}U$ | 1σ | $^{207}Pb/^{206}Pb$ | 1σ | $^{206}Pb/^{238}U$ | 1σ |
| 71006-21 | 17.0 | 435.0 | 0.04 | 0.06 | 0 | 0.73 | 0.02 | 0.09 | 0 | 555 | 29 | 559 | 7 |
| 71006-22 | 395.1 | 549.4 | 0.72 | 0.08 | 0 | 2.23 | 0.05 | 0.2 | 0 | 1180 | 23 | 1196 | 13 |
| 71006-23 | 76.4 | 130.8 | 0.58 | 0.21 | 0.01 | 14.52 | 0.33 | 0.5 | 0.01 | 2916 | 43 | 2607 | 27 |
| 71006-24 | 176.1 | 369.5 | 0.48 | 0.06 | 0 | 0.77 | 0.02 | 0.09 | 0 | 573 | 31 | 580 | 7 |
| 71006-25 | 150.0 | 711.6 | 0.21 | 0.06 | 0 | 0.72 | 0.02 | 0.09 | 0 | 592 | 28 | 542 | 6 |
| 71006-26 | 113.4 | 146.7 | 0.77 | 0.07 | 0 | 1.8 | 0.05 | 0.18 | 0 | 1040 | 34 | 1046 | 12 |
| 71006-27 | 378.2 | 727.4 | 0.52 | 0.07 | 0 | 1.46 | 0.03 | 0.15 | 0 | 925 | 24 | 911 | 10 |
| 71006-28 | 58.4 | 269.3 | 0.22 | 0.06 | 0 | 0.86 | 0.02 | 0.1 | 0 | 630 | 36 | 631 | 7 |
| 71006-29 | 268.7 | 188.1 | 1.43 | 0.06 | 0 | 0.82 | 0.03 | 0.1 | 0 | 611 | 48 | 608 | 7 |
| 71006-30 | 963.8 | 947.9 | 1.02 | 0.06 | 0 | 0.64 | 0.01 | 0.08 | 0 | 573 | 30 | 488 | 6 |
| 71006-31 | 183.9 | 432.0 | 0.43 | 0.08 | 0 | 1.66 | 0.05 | 0.15 | 0 | 1170 | 63 | 915 | 10 |
| 71006-32 | 250.9 | 748.9 | 0.33 | 0.07 | 0 | 1.48 | 0.03 | 0.15 | 0 | 922 | 24 | 924 | 10 |
| 71006-33 | 25.0 | 362.8 | 0.07 | 0.16 | 0 | 10.49 | 0.21 | 0.47 | 0.01 | 2482 | 18 | 2475 | 25 |
| 71006-34 | 344.3 | 443.1 | 0.78 | 0.06 | 0 | 0.77 | 0.02 | 0.09 | 0 | 582 | 31 | 583 | 7 |
| 71006-35 | 154.6 | 334.4 | 0.46 | 0.17 | 0 | 11.39 | 0.23 | 0.49 | 0.01 | 2558 | 18 | 2553 | 25 |
| 71006-36 | 110.5 | 105.1 | 1.05 | 0.06 | 0 | 0.77 | 0.03 | 0.09 | 0 | 581 | 53 | 583 | 8 |
| 71006-37 | 65.9 | 122.1 | 0.54 | 0.07 | 0 | 1.45 | 0.05 | 0.15 | 0 | 915 | 43 | 910 | 11 |
| 71006-38 | 8.6 | 71.5 | 0.12 | 0.06 | 0 | 1.06 | 0.04 | 0.12 | 0 | 734 | 50 | 737 | 10 |
| 71006-39 | 490.1 | 423.2 | 1.16 | 0.1 | 0 | 2.88 | 0.06 | 0.22 | 0 | 1565 | 23 | 1260 | 14 |
| 71006-40 | 120.7 | 224.2 | 0.54 | 0.08 | 0 | 2.19 | 0.06 | 0.2 | 0 | 1188 | 35 | 1172 | 14 |
| 71006-41 | 90.3 | 360.3 | 0.25 | 0.13 | 0 | 2.7 | 0.08 | 0.15 | 0 | 2054 | 59 | 927 | 11 |
| 71006-42 | 131.7 | 615.5 | 0.21 | 0.08 | 0 | 1.91 | 0.05 | 0.18 | 0 | 1090 | 29 | 1084 | 12 |
| 71006-43 | 169.4 | 424.1 | 0.40 | 0.06 | 0 | 0.9 | 0.02 | 0.11 | 0 | 676 | 37 | 645 | 8 |
| 71006-44 | 2263.1 | 862.6 | 2.62 | 0.07 | 0 | 1.12 | 0.02 | 0.11 | 0 | 1063 | 25 | 664 | 8 |
| 71006-45 | 151.2 | 335.5 | 0.45 | 0.07 | 0 | 1.86 | 0.04 | 0.18 | 0 | 1066 | 26 | 1067 | 12 |
| 71006-46 | 241.7 | 257.5 | 0.94 | 0.06 | 0 | 1 | 0.03 | 0.12 | 0 | 701 | 41 | 706 | 8 |
| 71006-47 | 136.7 | 241.3 | 0.57 | 0.08 | 0 | 2.61 | 0.06 | 0.22 | 0 | 1308 | 27 | 1301 | 14 |
| 71006-48 | 121.2 | 253.9 | 0.48 | 0.07 | 0 | 1.69 | 0.04 | 0.17 | 0 | 1009 | 33 | 1001 | 11 |
| 71006-49 | 186.9 | 297.9 | 0.63 | 0.14 | 0 | 6.9 | 0.15 | 0.37 | 0 | 2189 | 21 | 2008 | 21 |
| 71006-50 | 108.0 | 255.5 | 0.42 | 0.07 | 0 | 1.74 | 0.04 | 0.17 | 0 | 1025 | 28 | 1022 | 12 |
| 71006-51 | 352.2 | 438.4 | 0.80 | 0.07 | 0 | 1.45 | 0.03 | 0.15 | 0 | 903 | 30 | 913 | 10 |
| 71006-52 | 234.3 | 412.9 | 0.57 | 0.23 | 0 | 12 | 0.25 | 0.39 | 0 | 3023 | 19 | 2101 | 22 |
| 71006-53 | 38.7 | 682.4 | 0.06 | 0.16 | 0 | 10.51 | 0.22 | 0.47 | 0.01 | 2480 | 20 | 2483 | 25 |
| 71006-54 | 207.8 | 318.1 | 0.65 | 0.12 | 0 | 6.17 | 0.14 | 0.36 | 0 | 2001 | 22 | 2000 | 21 |
| 71006-55 | 733.1 | 1011.3 | 0.72 | 0.08 | 0 | 1.58 | 0.04 | 0.15 | 0 | 1104 | 27 | 900 | 10 |
| 71006-56 | 246.6 | 204.7 | 1.20 | 0.08 | 0 | 1.96 | 0.05 | 0.18 | 0 | 1207 | 31 | 1047 | 12 |
| 71006-57 | 258.2 | 647.8 | 0.40 | 0.08 | 0 | 2.01 | 0.05 | 0.19 | 0 | 1121 | 26 | 1118 | 12 |
| 71006-58 | 269.3 | 263.4 | 1.02 | 0.1 | 0 | 4.27 | 0.1 | 0.3 | 0 | 1691 | 24 | 1686 | 18 |
| 71006-59 | 133.0 | 314.0 | 0.42 | 0.07 | 0 | 1.85 | 0.04 | 0.18 | 0 | 1062 | 28 | 1063 | 12 |
| 71006-60 | 62.7 | 326.9 | 0.19 | 0.06 | 0 | 1.07 | 0.03 | 0.12 | 0 | 738 | 34 | 736 | 9 |
| 71006-61 | 175.5 | 527.1 | 0.33 | 0.07 | 0 | 1.71 | 0.04 | 0.17 | 0 | 1004 | 27 | 1015 | 11 |
| 71006-62 | 908.4 | 266.8 | 3.40 | 0.07 | 0 | 1.56 | 0.04 | 0.16 | 0 | 953 | 34 | 957 | 11 |
| 71006-63 | 299.3 | 510.4 | 0.59 | 0.06 | 0 | 0.77 | 0.02 | 0.09 | 0 | 591 | 36 | 574 | 7 |
| 71006-64 | 72.6 | 124.3 | 0.58 | 0.26 | 0.01 | 22.8 | 0.56 | 0.63 | 0.01 | 3258 | 22 | 3156 | 34 |
| 71006-65 | 109.8 | 321.6 | 0.34 | 0.09 | 0 | 2.7 | 0.08 | 0.22 | 0 | 1394 | 63 | 1287 | 15 |
| 71006-66 | 212.2 | 188.2 | 1.13 | 0.13 | 0 | 6.4 | 0.16 | 0.37 | 0 | 2035 | 26 | 2028 | 22 |
| 71006-67 | 57.5 | 54.2 | 1.06 | 0.17 | 0.01 | 10.02 | 0.36 | 0.44 | 0.01 | 2512 | 67 | 2348 | 29 |
| 71006-68 | 112.8 | 186.0 | 0.61 | 0.11 | 0 | 4.5 | 0.14 | 0.29 | 0 | 1830 | 63 | 1649 | 19 |
| 71006-69 | 247.2 | 208.4 | 1.19 | 0.08 | 0 | 2.32 | 0.06 | 0.21 | 0 | 1220 | 34 | 1217 | 14 |

| Spot number | Th (ppm) | U (ppm) | Th/U | Isotopic ratios | | | | | | Age (Ma) | | | |
|---|---|---|---|---|---|---|---|---|---|---|---|---|---|
| | | | | $^{207}Pb/^{206}Pb$ | 1σ | $^{207}Pb/^{235}U$ | 1σ | $^{206}Pb/^{238}U$ | 1σ | $^{207}Pb/^{206}Pb$ | 1σ | $^{206}Pb/^{238}U$ | 1σ |
| 71006-70 | 765.6 | 922.9 | 0.83 | 0.09 | 0 | 2.01 | 0.05 | 0.17 | 0 | 1350 | 27 | 1002 | 11 |
| 71006-71 | 62.2 | 100.0 | 0.62 | 0.06 | 0 | 0.9 | 0.05 | 0.1 | 0 | 671 | 94 | 643 | 9 |
| 71006-72 | 48.9 | 282.0 | 0.17 | 0.11 | 0 | 4.86 | 0.11 | 0.32 | 0 | 1793 | 25 | 1797 | 19 |
| 71006-73 | 52.5 | 323.7 | 0.16 | 0.19 | 0.01 | 11.64 | 0.27 | 0.43 | 0.01 | 2777 | 44 | 2328 | 24 |
| 71006-74 | 26.4 | 410.2 | 0.06 | 0.06 | 0 | 0.8 | 0.02 | 0.1 | 0 | 595 | 36 | 595 | 7 |
| 71006-75 | 194.3 | 272.3 | 0.71 | 0.06 | 0 | 0.66 | 0.02 | 0.08 | 0 | 514 | 42 | 515 | |

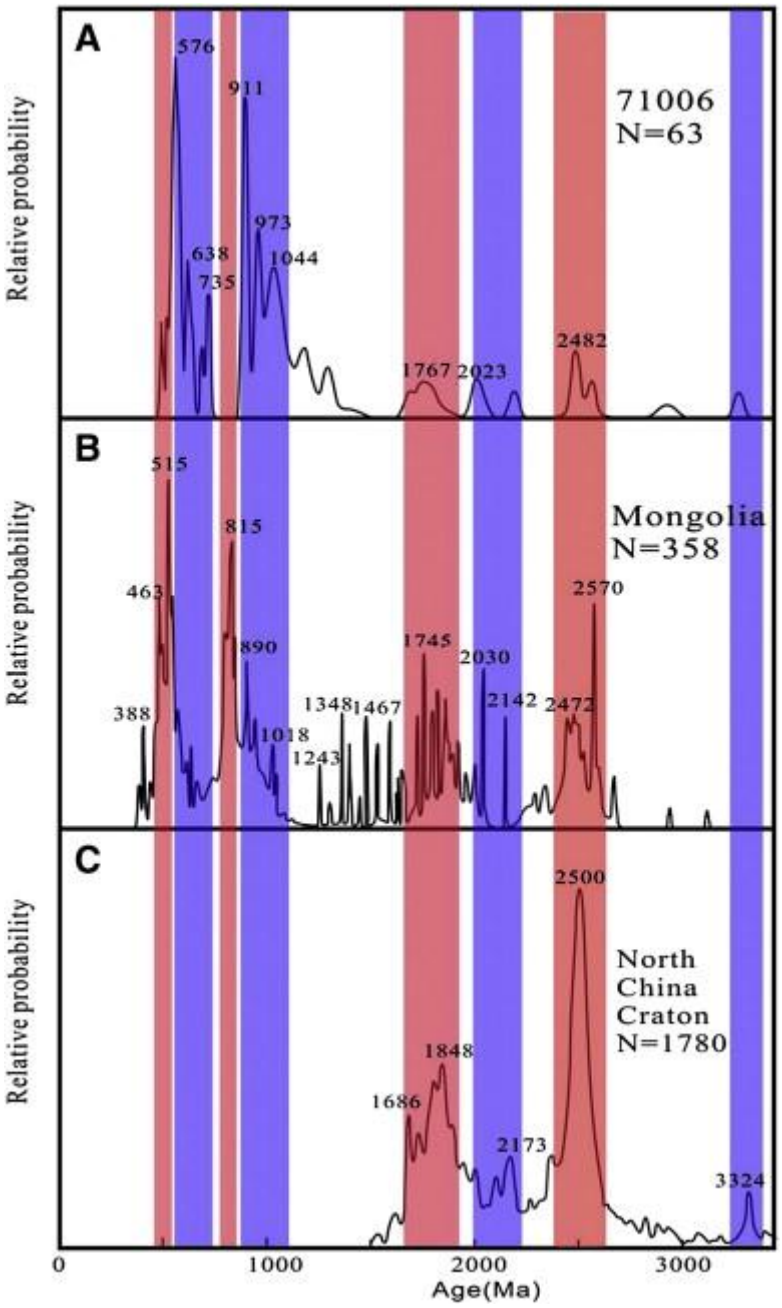


Fig. 16. Comparison of probability plots for 71006, Mongolia, NCC (compiled from Rojas-Agramonte et al., 2011 and this study).

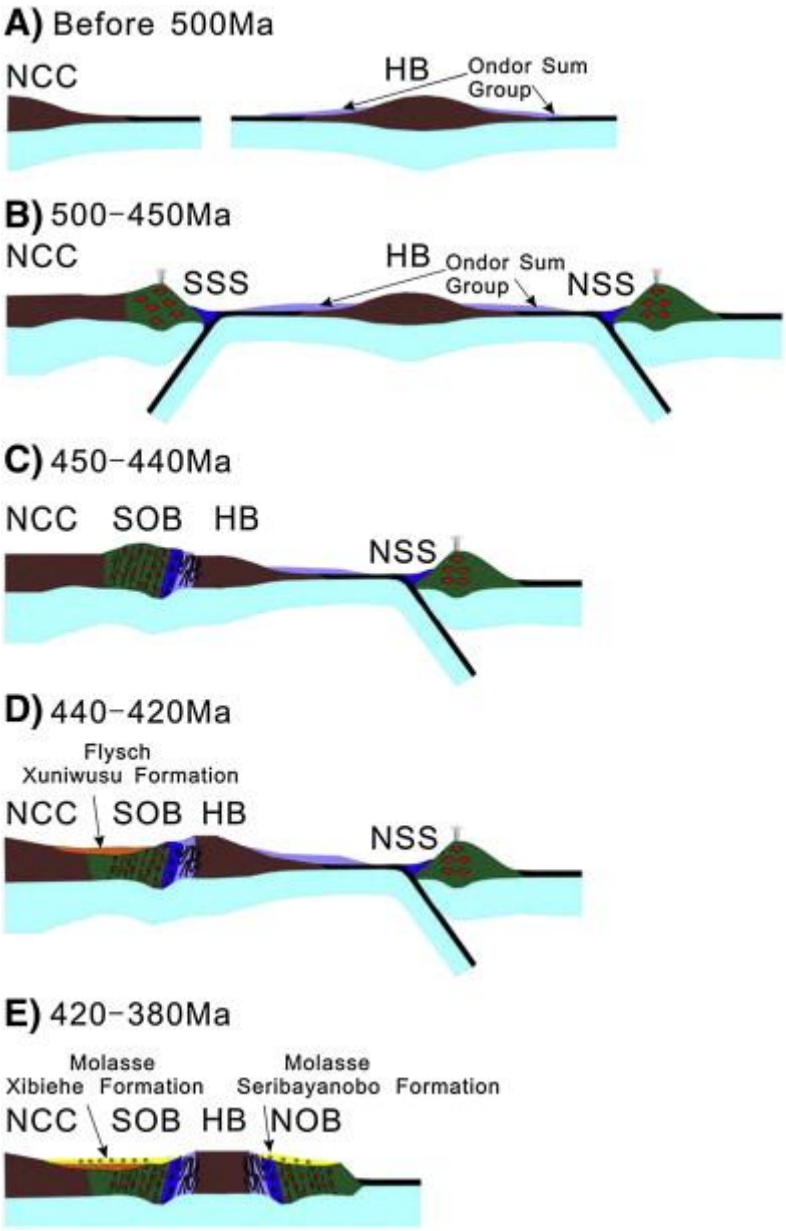


Fig. 17. Schematic geodynamic evolutionary model of the NOB and SOB in Inner Mongolia. SSS: southern subduction system; NSS: northern subduction system. NCC: North China Craton; HB: Hunshandake block; NOB: Northern Orogenic Belt, SOB: Southern Orogenic Belt.